Reliability-based assessment of LTF and CLT shear walls under in plane seismic loading using a modified Bouc-Wen hysteresis model

Angelo Aloisio[1], Francesco Boggian[2], Roberto Tomasi[3], and Massimo Fragiacomo[4]

[1]Research fellow. Università degli Studi dell'Aquila, via Giovanni Gronchi 18, 67100 L'Aquila, Italy. Email: angelo.aloisio1@univaq.it
[2]PhD student. University of Trento, via Mesiano 77, 38123 Trento, Italy. Email: francesco.boggian@unitn.it
[3]Professor. Norwegian University of Life Sciences, Campus Ås Drøbakveien 31, 1430 Ås, Norway. Email: roberto.tomasi@nmbu.no
[4]Professor. Università degli Studi dell'Aquila, via Giovanni Gronchi 18, 67100 L'Aquila, Italy. Email: massimo.fragiacomo@univaq.it

ABSTRACT

This paper reports the reliability-based assessment of Light Timber Frame (LTF) and Cross Laminated Timber (CLT) shear walls. The outcomes of cyclic tests on seventeen timber shear wall specimens calibrate the parameters of a modified Bouc-Wen model (Extended-Energy-dependent-Generalized-Bouc-Wen), obtained from the extension of the Generalized Bouc-Wen (GBW) model. The EEGBW model, which is alternative to the Bouc–Wen–Baber–Noori (BWBN) one, accurately, simulates the essential features of timber connections and structural systems. The EEGBW model, representative of the global response of the shear wall, expresses the resisting term of a Single-Degree of Freedom dynamic system, which describes the seismic response of a lumped mass supported by the shear walls. The results of truncated incremental dynamic analysis in terms of maximum displacement lead to the failure probabilities associated with increasing intensity measures. The resulting failure probabilities, fitted by a lognormal probability function, deliver the so-called fragility functions of the seventeen structural archetypes by assuming three different mass values. The failure probabilities return the estimation of the reliability indexes, which quantitatively assess the seismic reliability of the considered structures. Additionally, the authors discuss the role of the top mass and its effects upon the shear walls seismic performance by comparing the LTF and CLT structural systems.

INTRODUCTION

The use of timber in construction is widespread from ancient times, and nowadays, the most used structural systems for residential housing are Light Timber Frame (LTF)

and Cross-Laminated Timber (CLT). LTF structures represent most of the residential stock in the United States and Canada and are widely diffuse in the northern countries of Europe. LTF shear walls consist of sheathing panels, usually made by oriented strand board (OSB) or gypsum fibreboard (GFB), fastened by nails or staples to framing members along the perimeter. Lateral forces induced into the wall are resisted primarily by the sheathing and then transferred to the framing members via the connections. The entire wall assembly is then attached to the underlying structure using metal plates fastened to the wall itself and the floors, such as hold-downs and angle brackets or dowel type fasteners in the bottom rail, in order to ensure a continuous load path throughout the structure and adequate resistance against overturning and sliding actions. CLT is a new type of engineered wood product, developed in Europe, which has gained lots of popularity in recent decades (Brandner 2013; Aloisio et al. 2020c). It is usually produced in plate-like shape and is constituted by multiple glued layers of juxtaposed boards, such that each layer has alternate orthogonal grain orientation. In CLT shear walls no additional panels or nailing are required: the CLT itself has sufficient in-plane strength and stiffness. The connection to the underlying structure follows the same methods also used for LTF.

The design reliability of timber structures is traditionally achieved by deterministic methods using partial safety factors. However, in recent years, there is considerable interest in assessing the structural capacity via probabilistic methods (Gardoni et al. 2002). The estimation of the failure domain of many structural systems, like timber shear walls, may be hindered by the difficulties in modelling complicated hysteretic behaviours. The fragility functions, which relate the failure probability to a given intensity measure, like the Peak Ground Acceleration (PGA), require the outputs of nonlinear dynamic analysis and the consequent simulation of the shear walls seismic response.

Many scholars devoted their research to solve the modelling issues of timber shear walls or structural assemblies. Accurately, the hysteresis behaviour of timber shear walls is characterized by considerable stiffness, strength degradation and pinching, whose neglection yields unconservative results. Most of the scholars attempted to simulate the hysteresis of timber structures by using so-called empirical hysteresis models: they are mathematical models which lack direct physical meaning but closely match with the experimental cyclic tests.

In particular, Foliente (Foliente 1995) developed a very successful empirical model for timber structures. It is a general hysteresis model for single-degree-of-freedom (SDOF) systems based on a modification of the Bouc-Wen-Baber-Noori model. To the authors' knowledge, in the last ten years, significant achievements about empirical hysteresis models were made by Rinaldin et al. (Rinaldin et al. 2013) and Aloisio et al. (Aloisio et al. 2020b). Rinaldin et al. (Rinaldin et al. 2013) implemented a component approach for modelling the connections in cross-laminated wooden structures using an external subroutine in the Abaqus software package.

In 2020, following the work by Foliente, Aloisio et al. (Aloisio et al. 2020b) extended the Generalized Bouc-Wen model by (Song and Der Kiureghian 2006) to timber connections. The advantage of this analytical model mainly stands in the automatic parameter estimation based on a Least-Squares procedure described in (Aloisio et al. 2020b; Aloisio et al. 2019).

In this paper, the authors calibrated the modified Generalized Bouc-Wen model to the experimental tests on LTF and CLT shear walls characterized by the same geometry. Grossi et al. (Grossi et al. 2015) and Endrizzi (Endrizzi 2012) carried out experimental tests on LTF and CLT shear walls, presented in Section 3. The shear walls, modelled as Single-Degree-of-Freedom (SDOF) systems, consist of a top mass and an equivalent nonlinear spring (Section 4). The results of incremental nonlinear dynamic analysis lead to the fragility function estimation, by assuming the failure displacement equal to the ultimate displacement observed during the experimental tests (Section 3). The final section discusses the numerical outcomes.

BACKGROUND

In 2004, John W. van de Lindt defined the state-of-art about testing, modelling and reliability analysis of timber shear walls (Van De Lindt 2004). Despite the numerous experimental campaigns (almost 32 experimental campaigns in almost 20 years, from 1983 to 2004), few studies centred the reliability-based assessment of the performance of timber shear walls. The limited number of studies on this topic mainly derives from the difficulties in modelling the nonlinear dynamic behaviour of shear walls: Ceccotti and Foschi (Ceccotti and Foschi 1999) determined the design factor using a First-Order-Reliability-Method (FORM) based on a piece-wise linear hysteresis model (Ceccotti and Vignoli 1989). Foliente et al. (Foliente et al. 2000; Kasal et al. 1999) estimated the shear walls response using a modified Bouc-Wen-Baber-Noori (BWBN) model. Rosowsky (Rosowsky 2002) presented a risk-based methodology for the seismic design of timber shear walls. In 2003, Van de Lindt and Walz (van de Lindt and Walz 2003) investigated the seismic reliability of a wood shear wall at three sites around the United States using a polynomial backbone hysteresis model.

In the last fifteen years (2005-2020), there was still unbalance between the number of experimental tests on shear walls and reliability analysis on their seismic performance. As remarked by (Kirkham et al. 2014) in a 2014 review, the experimental investigation on shear walls testing progressed from static to dynamic and full-scale tests.

They (Kirkham et al. 2014) counted almost 20 studies about experimental tests on timber shear walls in ten years 2004-2014. To the authors' knowledge, few studies assessed the reliability of timber shear walls to hazards such as earthquake, wind, snow and fire (Vaidogas and Juocevičius 2008).

Specifically, the main findings concerning the fragility to seismic events are the followings.

In 2004, Ellingwood et al. (Ellingwood et al. 2004) assessed the fragility of light-frame wood construction subjected to wind and earthquake hazards, modelled as isolated subassemblies using CASHEW (Cyclic Analysis of SHEar Walls), a program developed as part of the CUREE-Caltech Wood Frame Project (Folz and Filiatrault 2001);

In 2007, Ellingwood et al. (Ellingwood et al. 2004) developed fragility models of light-frame wood structures using the program OpenSees (Open System for Earthquake Engineering Simulation, http://opensees.berkeley.edu) and the same CASHEW model;

In 2014 Gu (Gu 2014) estimated the seismic reliability of timber shear walls by considering the uncertainties from ground motion records, intensity measure, and resistance. The dynamic behaviour of the shear wall was simulated with a single-degree-of-freedom

(SDOF) system subject to ground shaking with a nonlinear spring representing the hysteretic behaviour (Foliente 1995).
In 2016 Seim et al. (Seim et al. 2016), presented an extensive study on oriented strand boards (OSB) and gypsum fiberboards (GFB) as sheathing materials for light-frame wall elements: the study spanned from cyclic testing to the seismic fragility estimation. In this paper, the authors estimate the seismic reliability of seventeen timber shear walls (Grossi et al. 2015) using the EEGBW model (Aloisio et al. 2020b).

EXPERIMENTAL CAMPAIGN: SETUP AND MAIN RESULTS

The focus of the present paper originates from the experimental data on LTF and CLT shear wall tests performed in the University of Trento and presented by (Grossi et al. 2015) and (Endrizzi 2012), respectively. They experimented LTF and CLT shear walls with dimensions of 2.5×2.5 m, using monotonic and cyclic load paths. Fig.1(b) and Fig.2 illustrate the test setup, which follows EN 594 (UNI, 2011). They applied multiple vertical loads and used different types of hold-downs, angle brackets and sheathing.
The LTF shear walls have the following characteristics. The frame elements were C24, characterized by cross-sections reported in Fig.1(a). Two types of sheathing were used: OSB/3 and GFP, with nails or staples as fasteners. The spacing of the sheathing-to-framing fasteners was also varied, as indicated in Tab.1. Angle brackets or inclined screws provided restraint against sliding. Two different types of hold-down were also tested, along with a specimen without hold-downs.

The specimens are labelled according to the following nomenclature: "LTF/CLT label-L number", where the label refers to the configuration explained in Tab.1,3 and L identifies the vertical load in kN/m.

Table 1. Characteristics of the tested LTF shear walls.

Specimen LTF	**STD**	**2F**	**150**	**50/RG**	**50**	**SCREW**	**WHD**
Sheathing	OSB/3	GFB	OSB/3	OSB/3	OSB/3	OSB/3	OSB/3
Thickness [mm]	15	12,5	15	15	15	15	15
Fastener type	Ring nails	Staples	Ring nails	Ring nails	Ring nails	Ring nails	Ring nails
⌀ [mm]	2.8	1.4x1.6	2.8	2.8	2.8	2.8	2.8
l [mm]	60	55	60	60	60	60	60
Perimeter spacing [mm]	100	100	150	50	50	100	100
Sliding restraint	New150	New150	New150	New150	New150	HBS	New150
n°	4	4	4	4	4	/	4
Fastener type	Anker nails	Anker nails	Anker nails	Anker nails	Anker nails	Screws	Anker nails
n°	12	12	12	12	12	25	12
⌀ [mm]	4	4	4	4	4	8	4
l [mm]	60	60	60	60	60	180	60
Uplift restraint	WHT340	WHT340	WHT340	WHT620	WHT340	WHT340	/
n°	2	2	2	2	2	2	/
Fastener type	Anker nails	Anker nails	Anker nails	Anker nails	Anker nails	Screws	/
n°	20	20	20	52	20	20	/
⌀ [mm]	4	4	4	4	4	4	/
l [mm]	60	60	60	60	60	60	/

Tab.2 summarizes the primary outcomes of the cyclic tests, which are the basis for further analysis in this paper. Fig.4 and Fig.5 present the results in the form of hysteresis loops, force and dissipated energy. Conversely, the CLT shear walls consist of three

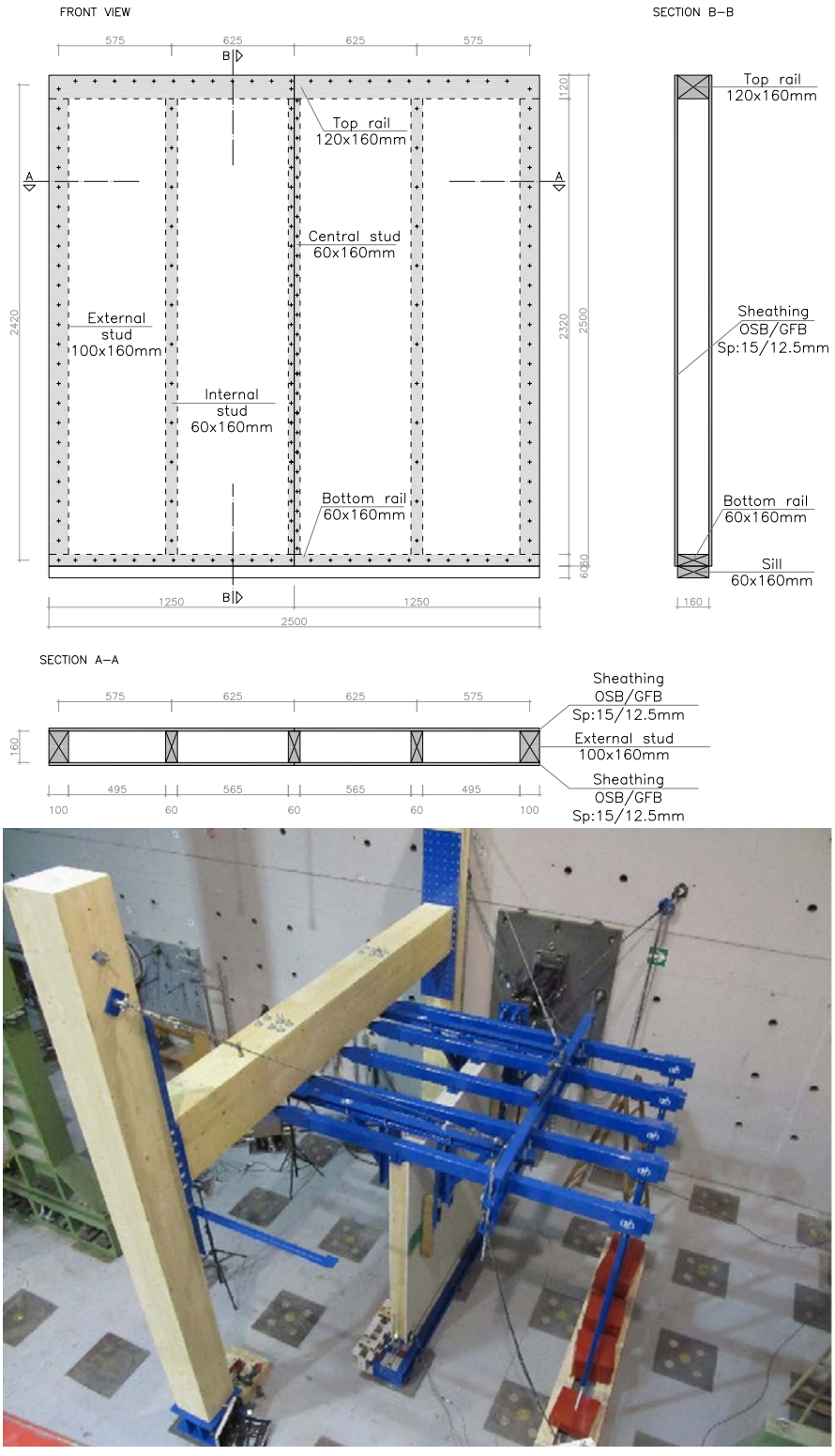

Fig. 1. (a) LTF specimen and (b) LTF test setup.

Table 2. Cyclic test results: F_u, ultimate experimental racking load; v_u, slip corresponding to the ultimate load; both evaluated according to EN12512.

LTF			CLT		
Test	F_u [kN]	v_u [mm]	**Test**	F_u [kN]	v_u [mm]
STD-L0	47.6	60.6	STD-L0	55.6	42.2
STD-L10	58.1	78.4	STD-L20	80.2	43.3
STD-L20	57.5	74.5	NA620-L0	124.0	29.1
2F-L20	38.9	33.5	NA620-L20	146.5	28.6
150-L20	49.6	70.8	ND620-L0	132.9	30.4
50/RG-L20	97.6	76.0	ND620-L20	160.5	32.6
50-L20	65.5	53.5	NA340-L20	83.6	57.4
SCREW-L20	57.6	74.9	NAWH-L20	66.6	57.7
WHD-L10	34.0	54.1			

layers (thickness 30-30-30 mm) made by C24 boards. As in the previous case, Endrizzi (Endrizzi 2012) experimented various vertical loads and different connection layouts: specifically, three different types of angle brackets to prevent sliding, two types of hold-down, along with a specimen without hold-downs. Tab.2 shows the main outcomes of the cyclic tests on CLT walls. Fig.6 and Fig.7 bestow the results in the form of hysteresis loops, force, dissipated energy.

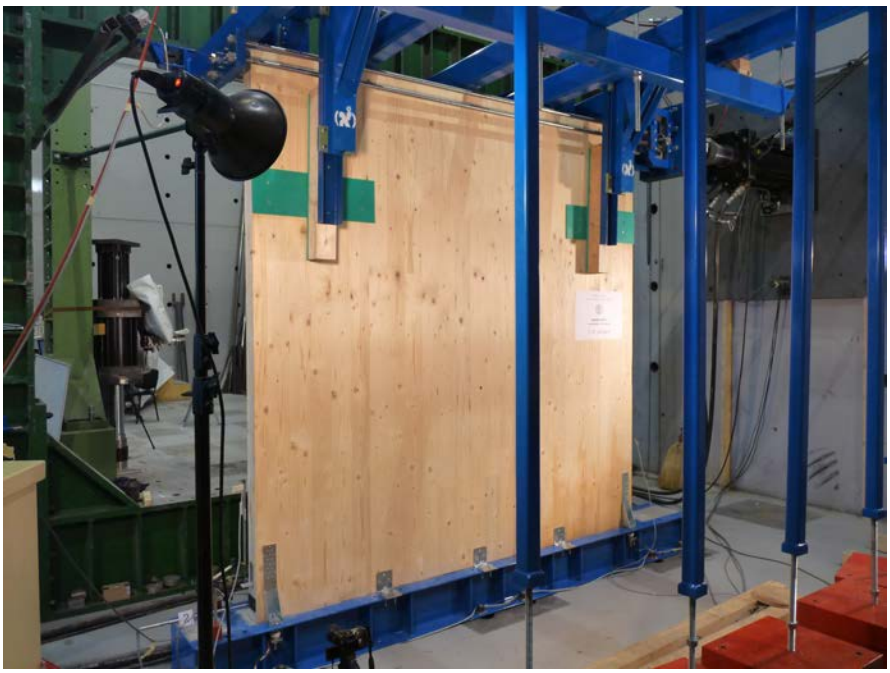

Fig. 2. CLT test setup

CALIBRATION OF THE MODIFIED BOUC-WEN MODEL

Table 3. Characteristics of the tested CLT shear walls.

Specimen CLT	**STD**	**NA620**	**ND620**	**NA340**	**NAWH**
Sliding restraint	100CR	10060newA	10060newD	10060newA	10060newA
n°	3	3	3	3	3
Fastener type	Anker nails	Anker nails	Anker nails	Anker nails	Anker nails
n°	12	30	30	30	30
⌀ [mm]	4	4	4	4	4
l [mm]	60	60	60	60	60
Uplift restraint	WHT340	WHT620	WHT620	WHT340	/
n°	2	2	2	2	/
Fastener type	Anker nails	Anker nails	Anker nails	Anker nails	/
n°	20	52	52	20	/
⌀ [mm]	4	4	4	4	/
l [mm]	60	60	60	60	/

The modified Generalized Bouc-Wen model, labelled as EEGBW (Extended-Energy-dependent-Generalized-Bouc-Wen), delivers an empirical representation of complex constitutive laws (Fig.3(b)), in particular, that of a timber shear wall, where the coexistence of different resisting mechanisms makes a direct FEM approach a quite complicated task. The equation of motion of a timber shear wall described by an inelastic SDOF system using the Generalized Bouc-Wen model can be expressed as follows, Fig.3(a):

$$m\ddot{x} + c\dot{x} + f_s(x, \dot{x}, z) = -m\ddot{x}_g \tag{1}$$

m	Mass;
x	Displacement;
$\dot{x}$	Derivative of x with respect to time;
$\ddot{x}$	Double derivative of x with respect to time;
$f_s(x, \dot{x}, z)$	Resisting inelastic force;
z	Auxiliary variable that represents the inelastic behaviour.

The stabilizing effect of the vertical load applied during the experimental test is already considered in the resisting Bouc-Wen term ($f_s(x, \dot{x}, \ddot{x})$), since each experimental test corresponds to a specific configuration of the vertical load (L number). The following parametric analyses then consider the variation of the sole inertia mass m, while the stabilizing load is kept constant. The resisting inelastic force carries the nonlinear effects, which, according to the Bouc–Wen class model, may be written as:

$$f_s(x, \dot{x}, z) = \alpha k_0 x + (1 - \alpha) k_0 z \tag{2}$$

α	Post-to preyield stiffness ratio
k_0	Initial stiffness

The resisting inelastic force originates from two contributions: elastic, depending on the displacement x, and inelastic depending on the inelastic displacement z. The

evolution of z is determined by an auxiliary ordinary differential equation, which can be written in the following form:

$$\dot{z} = \dot{x}[A - |z|^n \psi(x, \dot{x}, z)] \tag{3}$$

$\dot{z}$	Derivative of z with respect to time;
A	Parameter controlling the scale of the hysteresis loops;
n	Parameter controlling the sharpness of the hysteresis loops;
$\psi(x, \dot{x}, z)$	Nonlinear function controlling other shape features of the hysteresis loops.

The ψ function of the EEGBW model is:

$$\begin{aligned}\psi = \theta[&\beta_1(\epsilon)sgn(\dot{x}z) + \beta_2(\epsilon)sgn(\dot{x}x) + \beta_3(\epsilon)sgn(xz) + \beta_4(\epsilon)sgn(\dot{x}) + \\ &+ \beta_5(\epsilon)sgn(z) + \beta_6(\epsilon)sgn(x) + \beta_7(\epsilon)\left(\frac{\theta^+}{\theta}\right) + \beta_8(\epsilon)\left(\frac{\theta^-}{\theta}\right)]\end{aligned} \tag{4}$$

$\beta_{i\in[1-6]}$	Song's shape-control parameters;
β_7	Pinching shape parameter, active when $x > 0$, $\dot{x} > 0$ and $z > 0$;
β_8	Pinching shape parameter, active when $x < 0$, $\dot{x} < 0$ and $z < 0$;
$\theta, \theta^+, \theta^-$	Sign functions time-history dependent defined in (Aloisio et al. 2020b).
ϵ	Dissipated hysteretic energy.

In this paper, piecewise functions define the βs. Each β function is described by 20 constant values reported in Tabs.8-9, obtained by dividing the cyclic test into 20 equally-spaced parts. Each value corresponds to a given interval of dissipated hysteretic energy. The n exponent and the pinching fraction q, defined by (Aloisio et al. 2020b), are set equal to 0.6 and 0.9 respectively.

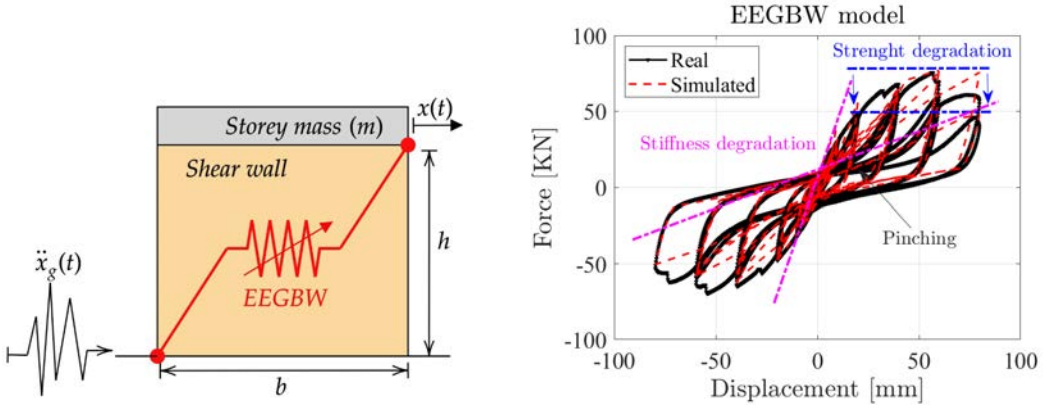

Fig. 3. (a) Shear wall modeling by an equivalent nonlinear spring, the EEGBW model; (b) Description of the main features of a EEGBW model.

Fig.4,5,6,7show the superposition between the experimental cyclic tests by (Grossi et al. 2015; Endrizzi 2012) and the EEGBW model in terms of force-displacement, force-time, and dissipated-energy-time curves. Despite there can be over or underestimation

of the dissipated hysteretic energy, there is an accurate correspondence in terms of displacement capacity, maximum resistance and pinched paths. This resemblance supports the use of these models as predictors of the particular shear walls behaviour and allows to attribute the differences in the simulated seismic response to the different constructive features.

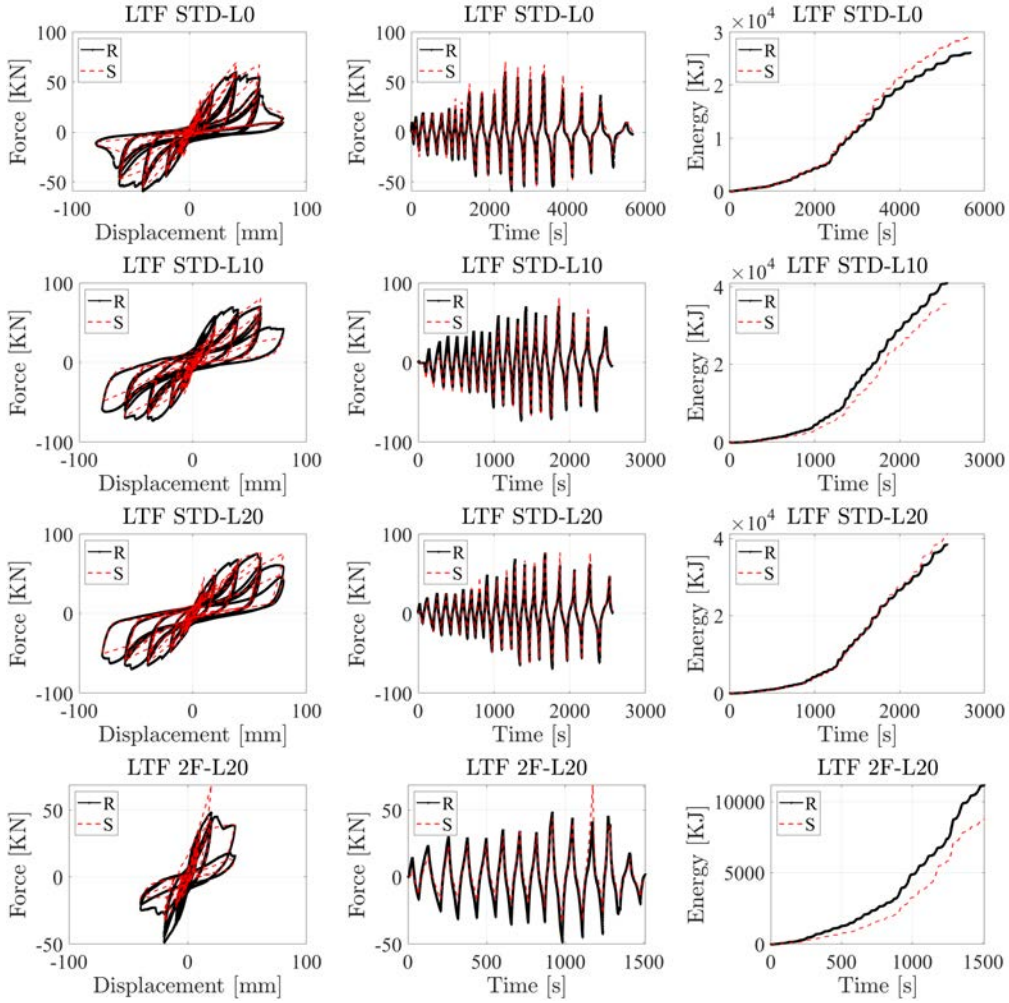

Fig. 4. LTF cyclic tests: superposition of the experimental results (R) and the identified EEGBW models (S) in terms of hysteresis loops, forces and dissipated energy.

NONLINEAR DYNAMIC ANALYSIS AND FRAGILITY FUNCTIONS ESTIMATION

The authors estimated the fragility functions of the shear walls from Truncated Incremental Dynamic Analysis (TIDA). The chosen control parameter is the maximum displacement attained during the seismic response. The exceeding of the ultimate displacement in Tab.2 identifies the failure domain. A lognormal function fits the failure probability values, following the algorithm presented by Baker (Baker 2015). The authors chose a set of Italian earthquake records to deal with the uncertainty from

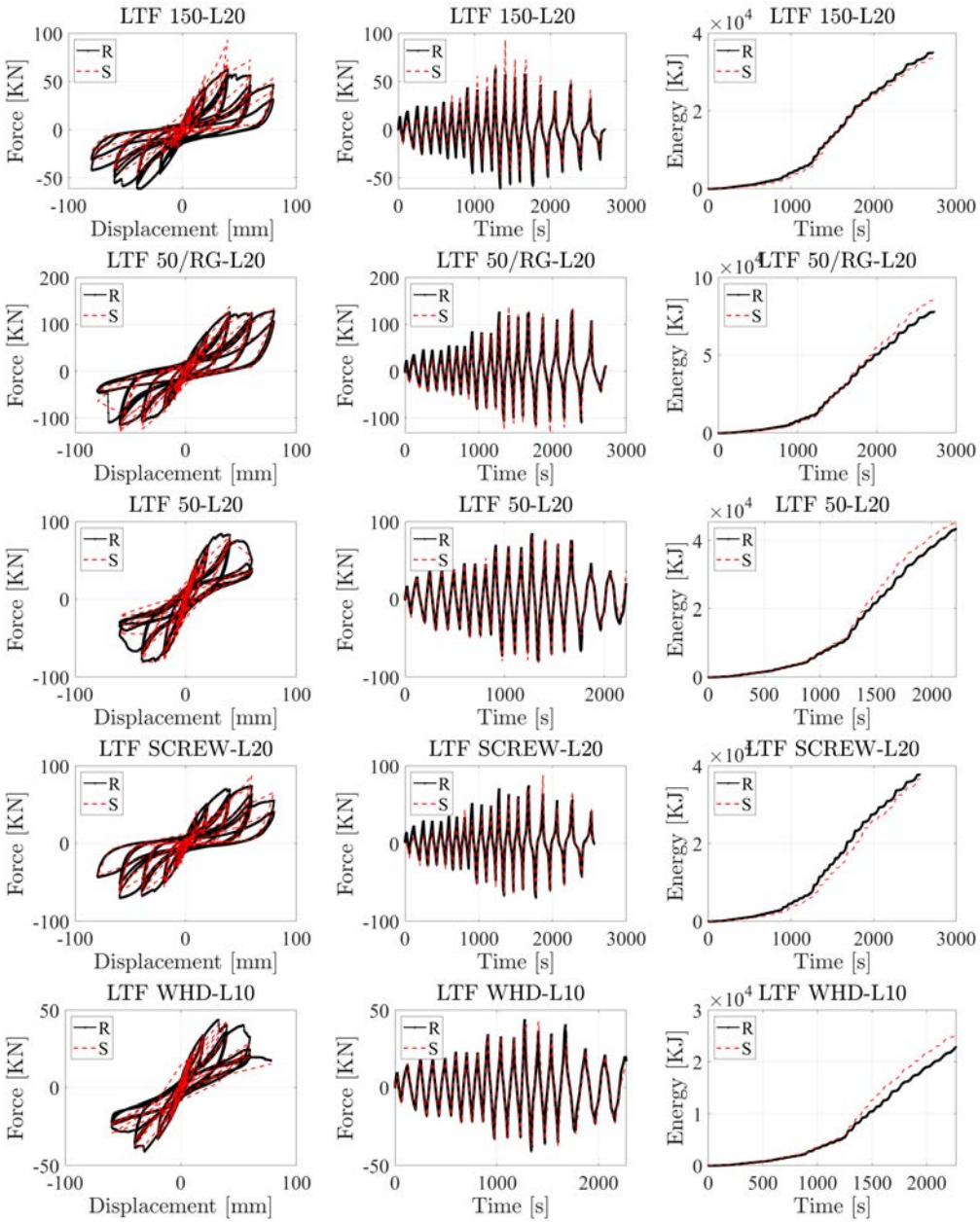

Fig. 5. LTF cyclic tests: superposition of the experimental results and the identified EEGBW models in terms of hysteresis loops, forces and dissipated energy.

the ground motion records. The earthquake records are homogenized to the same intensity level to yield consistent results from TIDA, and then they are optimized to match a given design spectrum, expected in L'Aquila (Italy) according to the national seismic code. The following subsections further feature three inherent aspects: the choice of the seismic hazard scenario, the estimation of the fragility functions and the determination of the reliability thresholds.

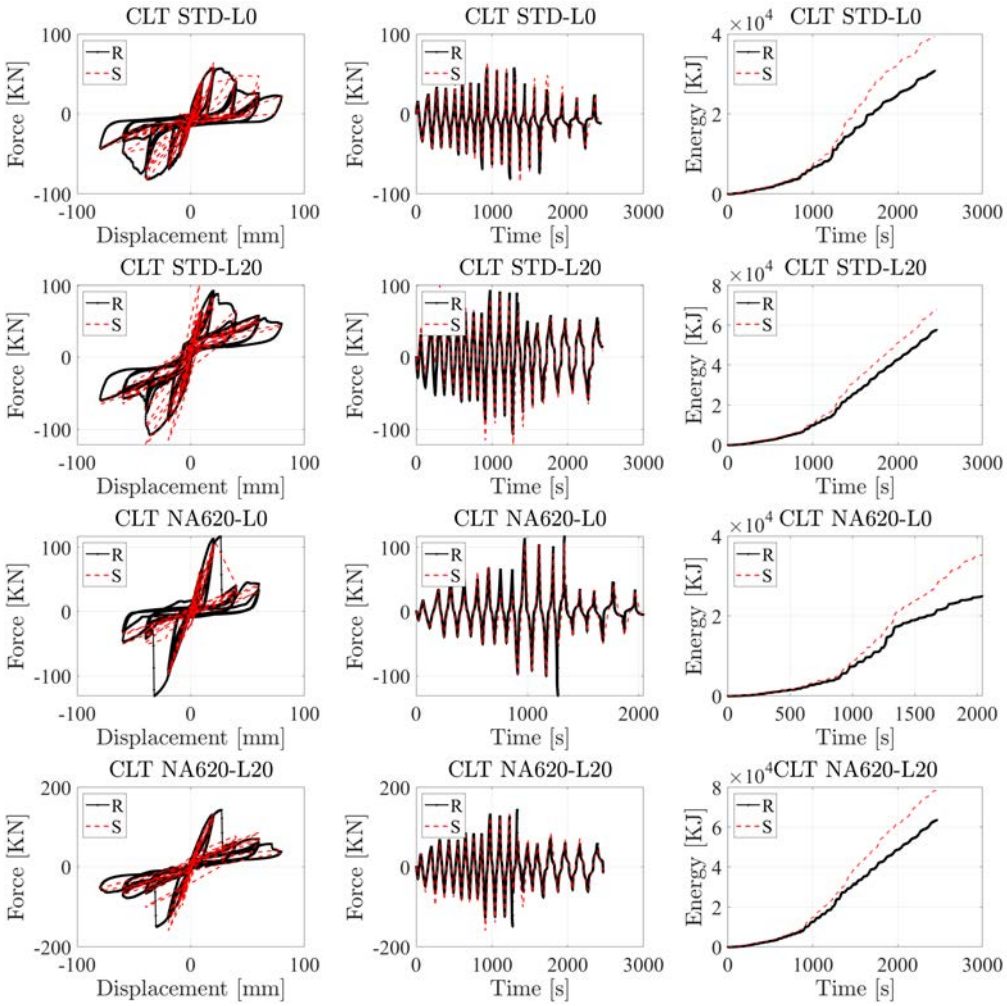

Fig. 6. CLT cyclic tests: superposition of the experimental results and the identified EEGBW models in terms of hysteresis loops, forces and dissipated energy.

Input: choice of earthquake records and fitting to the design spectrum

The list of 41 Italian earthquake records with magnitude ranging between 5 and 6.5, in Tab.7, represented the base for generating 41 artificial earthquakes, scaled to the same PGA and optimized to match the design spectrum in Fig.8 (Aloisio et al. 2020a). The 41 earthquakes correspond to all Italian earthquakes recorded since 1972 with PGA> 0.4g. A PGA exceeding 0.4–0.5g is related to severe damages to the structures in the Italian territory. Accordingly, the chosen PGA threshold became a "filter" for selecting the seismic scenario. The design spectrum corresponds to the seismic scenario expected in L'Aquila, Italy, according to the National Seismic Code. The algorithm presented by (Ferreira et al. 2020) is used to scale the accelerograms and carry out an Incremental Dynamic Analysis (IDA) based on coherent inputs, see Fig.8. The algorithm modifies the frequency content without producing substantial shape modifications. (Ferreira et al. 2020)

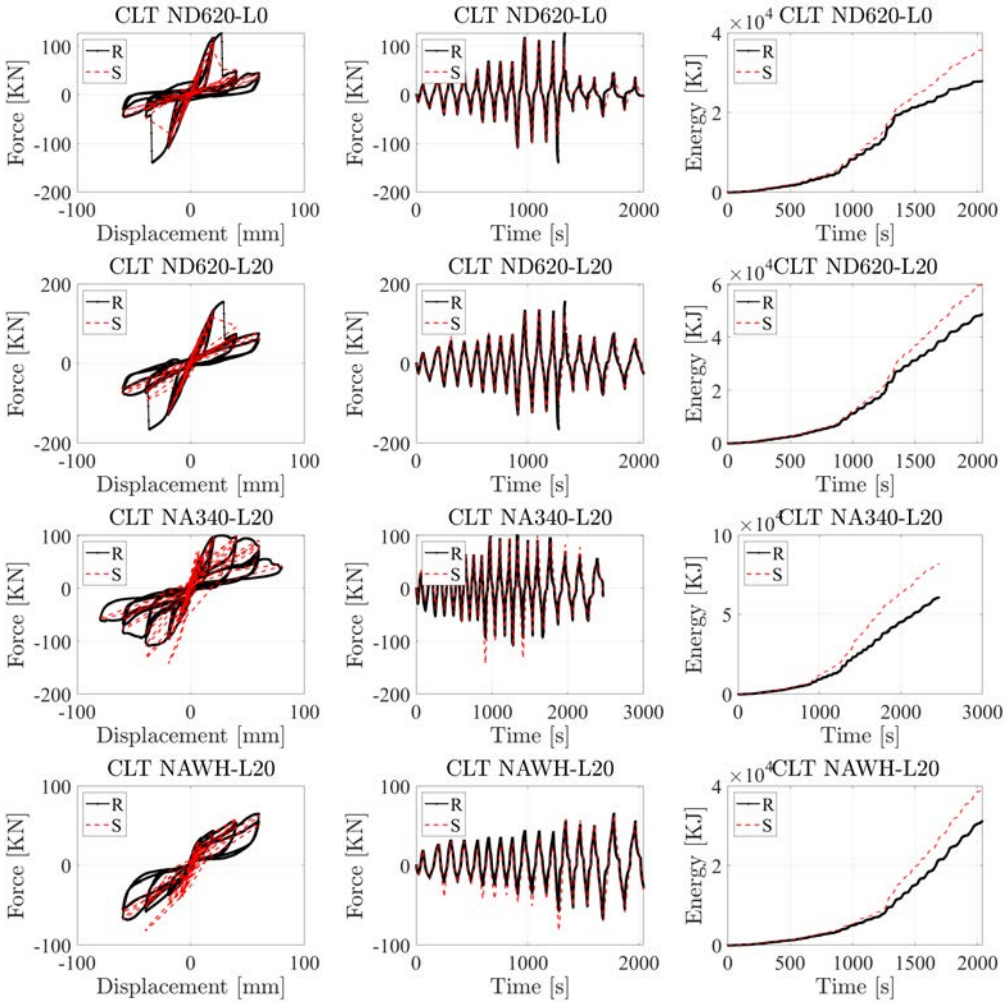

Fig. 7. CLT cyclic tests: superposition of the experimental results and the identified EEGBW models in terms of hysteresis loops, forces and dissipated energy.

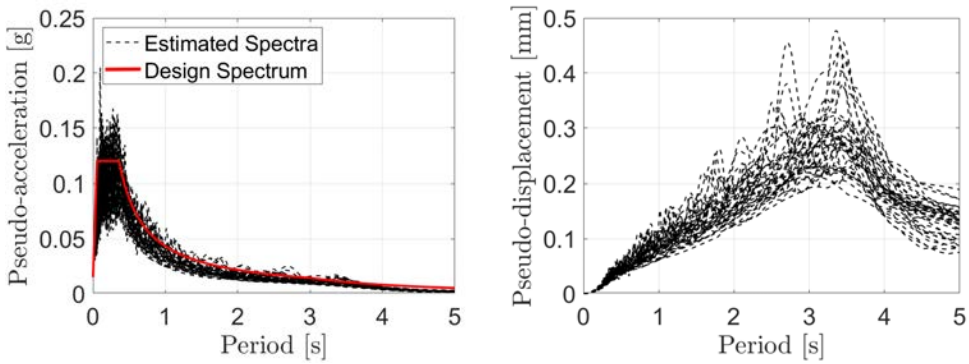

Fig. 8. Acceleration and displacement elastic spectra.

Fragility function

A lognormal cumulative distribution function fits the fragility function from data collected from NLDA (Baker 2015; Aloisio and Fragiacomo 2021):

$$P(C|IM = x) = \Phi\left(\frac{\ln(x/\theta)}{\beta}\right) \tag{5}$$

where $P(C|IM = x)$ represents the probability that a ground motion with intensity $IM = x$ causes the structure to collapse; Φ is the standard normal cumulative distribution function (CDF); θ is the median of the fragility function (the IM level with 50% probability of collapse); and β is the standard deviation of $\ln IM$. The TIDA leads to an alternative procedure (Baker 2015) to estimate the parameters θ and β, obtained by varying the parameters until maximizing a specific likelihood function. Specifically, the parameters are obtained by maximizing the logarithm of the following likelihood function:

$$\{\hat{\theta}, \hat{\beta}\} = \arg\max_{\hat{\theta},\hat{\beta}} \sum_{j=1}^{m} \left[\ln \Phi\left(\frac{\ln(IM_i/\theta)}{\beta}\right)\right] + [n-m]\ \ln\left[1 - \Phi\left(\frac{\ln(IM_{max}/\theta)}{\beta}\right)\right] \tag{6}$$

where $\hat{}$ denotes an estimated parameter, $\Phi()$ the standard normal PDF, n the number of ground motions used in the analysis, m the number of m ground motions that caused collapse at IM levels lower than IM_{max}, $\Phi()$ the standard normal CDF. The authors estimated the parameters of Eq.(6) for each of the 41 earthquake records. The resulting two parameters of the fragility function, representative of all considered seismic scenarios, are obtained taking the mean of all the couples of parameters estimated from each TIDA. Tab.10 displays the estimated parameters. The authors did not adopt alternative intensity measures other than the PGA. The choice of PGA as the intensity measure, rather than alternative measures (the Peak Spectral Acceleration, the Peak Ground Velocity or the Arias Intensity, e.g.), descends from the Italian seismic code, which classifies the seismic risk of the Italian territory according to the PGA levels.

Reliability threshold

The degree of reliability are defined by the standard EN 1990 (2002). The basic reliability targets for the ultimate limit state recommended in EN 1990 (2002) (Gulvanessian et al. 2002) are based on a semi-probabilistic approach, with the target value of reliability index β_d = 3.80 for a 50 years reference period, see Tab.4. The reliability

Table 4. Recommended minimum values of β_d and related failure probability P_f

Reliability class	β_d	P_f
RC3	4.3	8.50E-06
RC2	3.8	7.20E-05
RC1	3.3	4.80E-04

targets can be correctly derived from the failure probability. The reliability index (β_r) can be obtained from the failure probability $P(C|IM = x)$ by the following inversion:

$$\beta_r = \Phi\left(1 - P(C|IM = x)\right) \tag{7}$$

RESULTS

Fig.9 shows the fragility functions of the LTF and CLT shear walls for increasing values of the storey mass. These results enlighten the seismic performance of one-storey buildings, which are coarsely described by plane shear walls. The LTF and CLT shear walls exhibit very similar behaviour. The reasons for such similarity stem from the experimental cyclic curves, very similar in terms of capacity and shape of the hysteresis curves. The fragility of the considered structural archetypes rises as the inertia increases: this can be evidenced by a shift of the fragility functions towards the y-axis. The direct inspection of each figure confirms the same relations between the ultimate capacity of the shear walls reported in Tab.2. The reliability indexes in Eq.7 synthesize the discrepancies revealed by a macroscopic inspection of Fig.9. Fig.10 expands the initial portion of the fragility function associated with lower probability values. The seismic reliability decreases as the PGA increases. A dashed line corresponding to $\beta_d = 3.8$ intersects the reliability functions: the intersection points indicate the maximum PGA acceptable to yield the given reliability threshold. The reliability indexes decrease as the top mass increases: the reliability functions shift towards the y-axis, as shown in Fig.10.

Tab.5,6 synthesize the quantitative results from Fig.10. Additionally, Tab.5,6 may enlighten on a direct design problem, i.e. the assessment of the storey mass given a PGA value obtained from the local seismic hazard.

Given a PGA value, the function in Fig.11 delivers the maximum mass per unit of length tolerable by the shear wall to yield the given reliability threshold. This picture further remarks an essential feature: the top mass introduces opposing contributes to the equilibrium of the shear walls: the stabilizing moment and the inertia force. The values of Tab.5,6 corresponding to $L \approx mg$, prove that, averagely, the inertia contribution prevails over the stabilizing moment during a seismic event. For instance, considering LTF results in Tab.5, the doubling of both the top mass (m) and vertical load ($L \approx mg$) causes a profound decrease ($\frac{0.048}{0.213} \approx 0.23$) in the PGA values associated with $\beta_d = 3.8$.

Table 5. PGA [g] associated to the chosen reliability threshold $\beta_d = 3.8$ of LTF shear walls.

Test	**Storey mass LTF** [kg]		
	1000	1500	2000
LTF STD-L0	0.148	0.08	0.035
LTF STD-L10	0.213	0.102	0.068
LTF STD-L20	0.215	0.102	0.048
LTF 2F-L20	0.051	0.032	0.015
LTF 150-L20	0.193	0.106	0.051
LTF 50/RG-L20	0.215	0.102	0.061
LTF 50-L20	0.093	0.049	0.033
LTF SCREW-L20	0.215	0.102	0.061
LTF WHD-L10	0.123	0.047	0.031
Mean	0.163	0.082	0.045
St. dev.	0.062	0.030	0.017

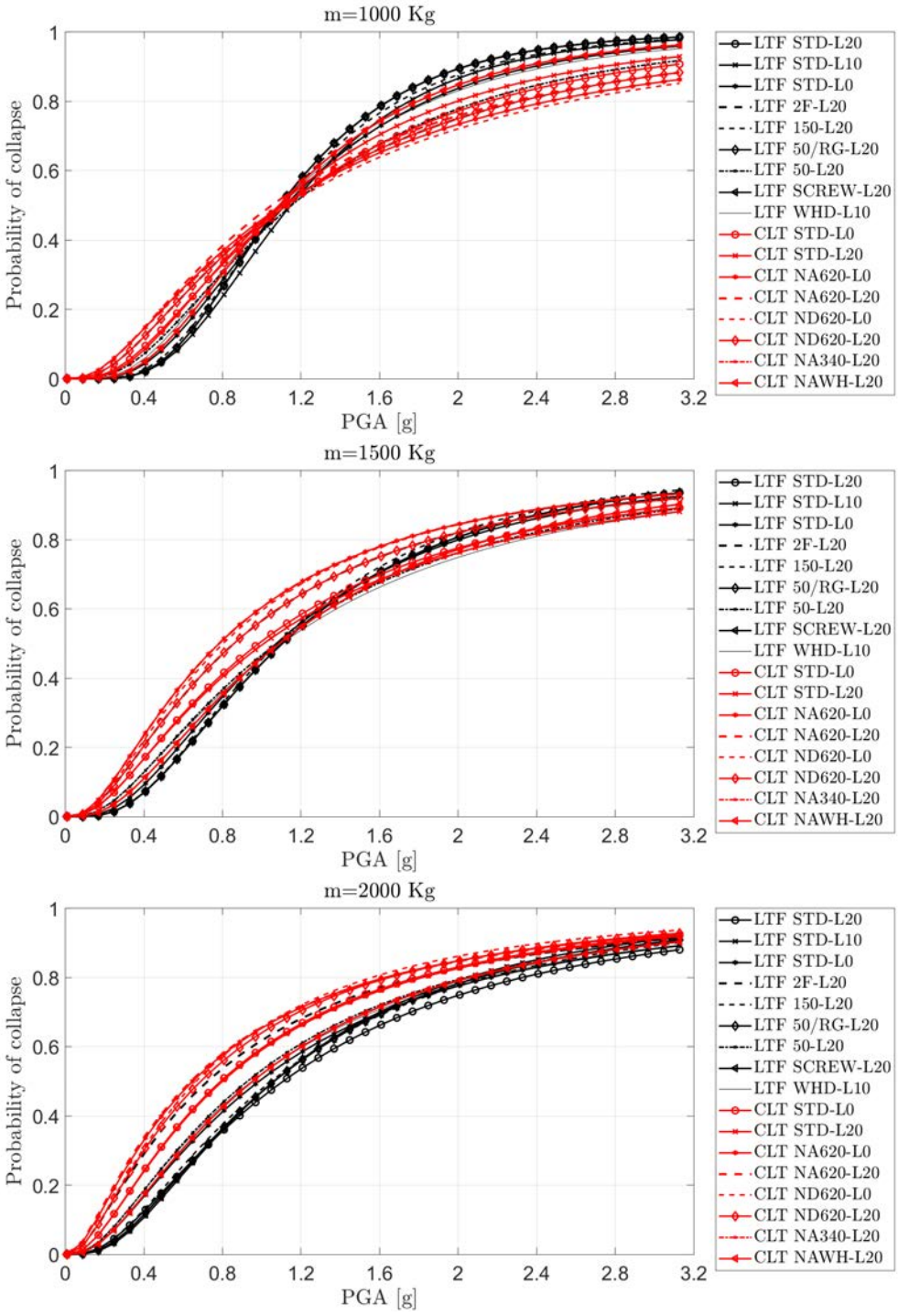

Fig. 9. Fragility functions of the considered shear walls models considering increasing values of the storey mass: 1000, 1500 and 2000 Kg, respectively.

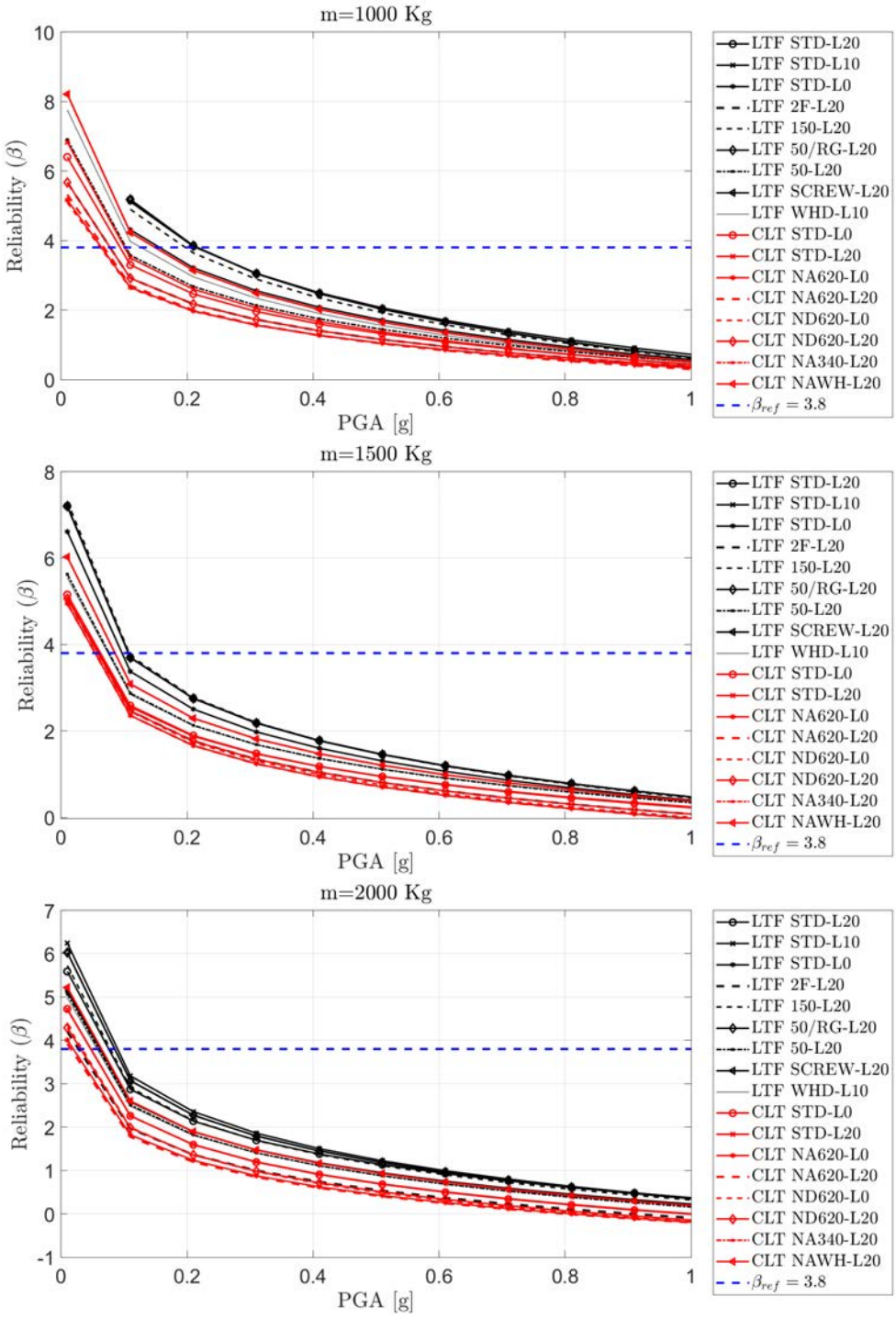

Fig. 10. Reliability functions of the considered shear walls models considering increasing values of the storey mass: 1000, 1500 and 2000 Kg, respectively.

Table 6. PGA [g] associated to the chosen reliability threshold $\beta_d = 3.8$ of CLT shear walls.

Test	**Storey mass CLT** [kg]		
	1000	1500	2000
CLT STD-L0	0.075	0.035	0.025
CLT STD-L20	0.088	0.033	0.024
CLT NA620-L0	0.037	0.029	0.013
CLT NA620-L20	0.04	0.029	0.011
CLT ND620-L0	0.035	0.032	0.018
CLT ND620-L20	0.051	0.032	0.017
CLT NA340-L20	0.142	0.061	0.037
CLT NAWH-L20	0.142	0.061	0.037
Mean	0.076	0.039	0.023
St. dev.	0.045	0.014	0.010

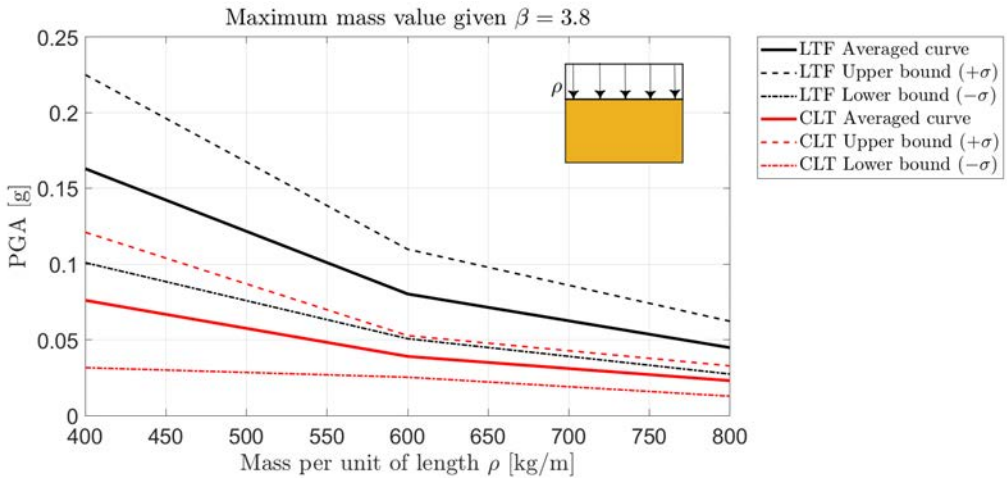

Fig. 11. PGAs associated to the top mass values given a reliability threshold $\beta = 3.8$.

DISCUSSION OF RESULTS

The hysteresis loops illustrated in Fig.4,5,6,7 manifest distinct trends in the global response of LTF and CLT shear walls. The pinching phenomenon is more pronounced in LTF shear wall tests, seemingly due to the sheathing-to-framing connections, made by metal dowel-type connections characterized by small diameters. They are largely used in this type of shear walls to fasten the perimeter of the sheathing. Stiffness degradation is also more evident and progressive in LTF cycles compared to CLT, suggesting, as expected, that the CLT panels retain more of their original stiffness as the cyclic loading advances.

This phenomenon is detectable from the curvature of the reloading branches of the loops, which present a deeper concavity in LTF tests. The overall behaviour of LTF shear walls is more ductile than CLT. Almost every CLT test manifests a sudden fall in

stiffness, due to the failure of the hold-downs; this implies that the behaviour of CLT walls is mainly attributable to the base connections.
The fragility functions, presented in Fig.9, confirm the mutual analogies of the considered structural systems under lateral loads: both structural assemblies are sufficiently stiff, and, accordingly, the base connections mainly drive the global response of the wall systems. Fig.10 conveys the same information, and the small differences beforehand underlined between LTF and CLT in hysteresis loops yield slightly higher reliability of LTF walls at each PGA level. The final assessment is the following: the testing of the walls is truly a test of their connections systems, and, if the structural assembly is stiff enough, as is the case, the two technologies LTF and CLT are not too dissimilar.
The unique significant difference is that the CLT walls averagely exhibit a more fragile response. The higher fragility depends on the considerable stiffness of the CLT panel compared to the LTF assembly. The base connections reach failure very early compared to the LTF case, thus approaching the global collapse with higher forces and smaller ultimate displacements, as marked in Tab.2.
As a summary of this difference, Fig.11 shows that, given the same reliability threshold, CLT walls present a minor admissible mass compared to LTF walls at a certain PGA level. For instance, with the same applied vertical load, the LTF wall withstands higher PGAs than the CLT wall. In the future, the authors will aim at exploring the role of the gradual loss of stiffness of the timber assemblies and the yielding local phenomena of timber material. The extension of the compressed area during the rocking motion of the panel affects sensibly the load transferred to the hold-downs. The investigation may lead to an elementary predictive capacity model capable of estimating the force on the hold-downs by using the available experimental data and numerical modelling.

CONCLUSIONS

The reliability-based assessment is increasing popularity, and several scholars attempt to design structures via probabilistic approaches. This paper estimates the failure probability of seventeen timber shear walls, nine Light-Timber Frame (LTF) and eight Cross-Laminated Timber (CLT), based on the extension of a generalized Bouc-Wen model. This model, labelled as Extended-Energy dependent Generalized Bouc-Wen model (EEGBW), closely reproduces the hysteretic behaviour of the tested specimens, characterized by pinching and both strength and stiffness degradation. The results of the truncated incremental dynamic analysis (TIDA) of a Single-Degree of Freedom (SDOF) oscillator represented by a lumped mass and a resisting term expressed by the EEGBW model roughly describes the in-plane seismic response of the considered shear walls. The resulting fragility functions fit the failure probabilities of the considered structural archetypes. The authors observed a distinguished similarity between the seismic performance of Light Timber Frame (LTF) and Cross-Laminated Timber (CLT) shear walls. Despite the inherent differences, the two structural systems manifest an analogue behaviour: both wall assemblies are sufficiently stiff, and thus the response of the wall systems mainly governed by its hold-down connections. The fragility functions confirm this evidence: the ones associated with LTF resemble those of CLT walls closely. Additionally, the authors noted that the inertia force related to the mass prevails over its stabilizing contribute in the equilibrium equations, indicating that the structural

archetypes' fragility increases as the inertia grows. This phenomenon is evident in CLT walls, which present a lower level of admissible mass, given the same PGA level and reliability threshold. Averagely, CLT walls exhibit a more fragile behaviour than LTF, due to their superior stiffness, which produces failure of the base connections earlier than LTF walls. The considered tested walls may not be entirely representative of a real structure, however, structural archetypes are very useful in illustrating the performance of structural systems, before the investigation of more complicated behaviours.

DATA AVAILABILITY STATEMENT

All data, models, or code that support the findings of this study are available from the corresponding author upon reasonable request.

ACKNOWLEDGEMENTS

The authors acknowledge the research efforts of Paolo Grossi, Paolo Endrizzi, Tiziano Sartori and Ermanno Acler, who carried out the experimental tests with the support of the staff of the University of Trento.

REFERENCES

Aloisio, A., Alaggio, R., and Fragiacomo, M. (2019). "Dynamic identification of a masonry façade from seismic response data based on an elementary ordinary least squares approach." *Engineering Structures*, 197, 109415.

Aloisio, A., Alaggio, R., and Fragiacomo, M. (2020a). "Fragility functions and behavior factors estimation of multi-story cross-laminated timber structures characterized by an energy-dependent hysteretic model." *Earthquake Spectra*, 8755293020936696.

Aloisio, A., Alaggio, R., Köhler, J., and Fragiacomo, M. (2020b). "Extension of generalized bouc-wen hysteresis modeling of wood joints and structural systems." *Journal of Engineering Mechanics*, 146(3), 04020001.

Aloisio, A. and Fragiacomo, M. (2021). "Reliability-based overstrength factors of cross-laminated timber shear walls for seismic design." *Engineering Structures*, 228, 111547.

Aloisio, A., Pasca, D., Tomasi, R., and Fragiacomo, M. (2020c). "Dynamic identification and model updating of an eight-storey clt building." *Engineering Structures*, 213, 110593.

Baker, J. W. (2015). "Efficient analytical fragility function fitting using dynamic structural analysis." *Earthquake Spectra*, 31(1), 579–599.

Brandner, R. (2013). "Production and technology of cross laminated timber (clt): A state-of-the-art report." *Focus Solid Timber Solutions - European Conference on Cross Laminated Timber (CLT)*, University of Bath, 3–36.

Ceccotti, A. and Foschi, R. O. (1999). "Reliability assessment of wood shear walls under earthquake excitation." *Proc., 3rd Int. Conf. on Computational Stochastic Mechanics, Balkema, Brookfield, VT*, 311–317.

Ceccotti, A. and Vignoli, A. (1989). "A hysteretic behavioural model for semi-rigid joints." *European Earthquake Engineering*, 3, 3–9.

Ellingwood, B. R., Rosowsky, D. V., Li, Y., and Kim, J. H. (2004). "Fragility assessment of light-frame wood construction subjected to wind and earthquake hazards." *Journal of Structural Engineering*, 130(12), 1921–1930.

Endrizzi, P. (2012). "I sistemi di connessione di base del pannello xlam compensato di tavole: indagine sperimentale in scala reale e modellazione numerica della capacità portante globale di parete ottenuta con l'impiego di una nuova tipologia di angolare a taglio." M.S. thesis, University of Trento, Italy.

Ferreira, F., Moutinho, C., Cunha, Á., and Caetano, E. (2020). "An artificial accelerogram generator code written in matlab." *Engineering Reports*, 2(3), e12129.

Foliente, G. C. (1995). "Hysteresis modeling of wood joints and structural systems." *Journal of Structural Engineering*, 121(6), 1013–1022.

Foliente, G. C., Paevere, P., Saito, T., and Kawai, N. (2000). "Reliability assessment of timber shear walls under earthquake loads." *Proc., 12th World Conf. on Earthquake Engineering (12WCEE)*.

Folz, B. and Filiatrault, A. (2001). "Cyclic analysis of wood shear walls." *Journal of structural engineering*, 127(4), 433–441.

Gardoni, P., Der Kiureghian, A., and Mosalam, K. M. (2002). "Probabilistic capacity models and fragility estimates for reinforced concrete columns based on experimental observations." *Journal of Engineering Mechanics*, 128(10), 1024–1038.

Grossi, P., Sartori, T., and Tomasi, R. (2015). "Tests on timber frame walls under in-plane forces: part 2." *Proceedings of the Institution of Civil Engineers-Structures and Buildings*, 168(11), 840–852.

Gu, J. (2014). "Seismic reliability analysis of wood shear walls using different methods." *Journal of Structural Engineering*, 140(2), 04013054.

Gulvanessian, H., Calgaro, J.-A., and Holickỳ, M. (2002). *Designer's guide to EN 1990: eurocode: basis of structural design*. Thomas Telford.

Kasal, B., Collins, M., Foliente, G. C., and Paevere, P. (1999). "A hybrid deterministic and stochastic approach to inelastic modeling and analysis of light-frame buildings." *Proc., 1st Int. RILEM Symp. on Timber Engineering*, 61–70.

Kirkham, W. J., Gupta, R., and Miller, T. H. (2014). "State of the art: Seismic behavior of wood-frame residential structures." *Journal of Structural Engineering*, 140(4), 04013097.

Rinaldin, G., Amadio, C., and Fragiacomo, M. (2013). "A component approach for the hysteretic behaviour of connections in cross-laminated wooden structures." *Earthquake engineering & structural dynamics*, 42(13), 2023–2042.

Rosowsky, D. V. (2002). "Performance of timber buildings under high wind loads." *Progress in Structural Engineering and Materials*, 4(3), 286–290.

Seim, W., Kramar, M., Pazlar, T., and Vogt, T. (2016). "Osb and gfb as sheathing materials for timber-framed shear walls: Comparative study of seismic resistance." *Journal of Structural Engineering*, 142(4), E4015004.

Song, J. and Der Kiureghian, A. (2006). "Generalized bouc–wen model for highly asymmetric hysteresis." *Journal of engineering mechanics*, 132(6), 610–618.

Vaidogas, E. and Juocevičius, V. (2008). "Reliability of a timber structure exposed to fire: estimation using fragility function." *Mechanics*, 73(5), 35–42.

Van De Lindt, J. W. (2004). "Evolution of wood shear wall testing, modeling, and reliability analysis: Bibliography." *Practice Periodical on Structural Design and Construction*, 9(1), 44–53.

van de Lindt, J. W. and Walz, M. A. (2003). "Development and application of wood

shear wall reliability model." *Journal of structural Engineering*, 129(3), 405–413.

APPENDIX A

Table 7. List of earthquake recordings sorted from largest to smallest PGA.

No	**Year**	**Location (Italy)**	**Epicentral distance** [km]	**PGA** [g]	**Depth** [km]	**ML**	**MW**
1	2016	Norcia	11.0	**0.931**	9.2	6.1	6.5
2	2016	Accumoli	8.5	**0.851**	8.1	6.0	6.0
3	2009	Fossa	3.6	**0.652**	17.1	5.4	5.5
4	2009	L'aquila	4.9	**0.644**	8.3	5.9	6.1
5	2016	Visso	7.1	**0.638**	7.5	5.9	5.9
6	1976	Lusevra	6.2	**0.632**	6.8	6.1	5.9
7	2009	Montereale	7.9	**0.550**	9.4	5.3	5.4
8	2012	Medolla	9.3	**0.495**	8.1	5.8	6.0
9	1976	Lusevra	27.7	**0.346**	5.7	6.4	6.4
10	1976	Gemona del friuli	16.2	**0.342**	11.3	6.0	6.0
11	1976	Friuli Venezia Giulia	9.4	**0.322**	4.3	5.8	5.6
12	1980	Laviano	33.3	**0.314**	15.0	6.5	6.9
13	2016	Castel Sant'Angelo sul Nera	9.4	**0.295**	8.1	5.4	5.4
14	2009	L'Aquila	11.0	**0.294**	11.0	5.1	5.4
15	2017	Cagnano amiterno	10.8	**0.289**	9.5	5.1	5.0
16	2009	L'Aquila	7.4	**0.264**	9.0	5.0	5.0
17	2012	Finale Emilia	16.1	**0.259**	9.5	5.9	6.1
18	2012	San Possidonio	6.9	**0.252**	7.2	5.1	5.5
19	1976	Nimis	7.0	**0.241**	13.3	5.5	5.1
20	1977	Trasaghis	7.1	**0.238**	10.8	5.3	5.3
21	2013	Fivizzano	11.9	**0.227**	7.0	5.2	5.1
22	2012	San Felice sul Panaro	7.4	**0.205**	5.0	5.1	9.1
23	1984	Perugia	20.6	**0.201**	6.0	5.2	5.6
24	2016	Norcia	4.4	**0.191**	8.0	5.4	5.3
25	1997	Foligno	20.1	**0.184**	5.5	5.4	5.4
26	1997	Foligno	21.6	**0.184**	5.7	5.8	6.0
27	2001	Naturno	25.9	**0.167**		5.3	4.8
28	1984	Villetta Barrea	17.4	**0.158**	12.1	5.7	5.5
29	1997	Foligno	24.2	**0.152**	5.7	5.6	5.7
30	2009	Pizzoli	10.1	**0.148**	9.7	5.0	5.1
31	1984	Settefrati	10.1	**0.110**	20.5	5.9	5.9
32	2012	Berceto	67.4	**0.098**	72.4	5.2	5.0
33	1990	Potenza	29.0	**0.096**	10.0	5.2	5.8
34	1997	Sellano	4.1	**0.082**	4.8	5.1	5.2
35	1978	Bruzzano Zeffirio	9.2	**0.076**	5.0	5.3	5.2
36	2004	Vobarno	13.6	**0.072**	5.4	5.2	5.0
37	2012	Mirabello	20.4	**0.070**	3.4	5.1	5.2
38	2002	Bonefro	38.1	**0.057**	13.0	5.4	5.7
39	2018	Molise	22.3	**0.045**	19.6	5.2	5.1
40	2002	Casacalenda	46.1	**0.032**	10.0	5.3	5.7
41	2008	Neviano degli Arduini	47.6	**0.022**	22.9	5.2	5.5

Table 8. Parameters of the EEGBW models corresponding to the LTF tests: the 20 values derive from division of the experimental data into 20 equal segments, named steps, characterized by constant β values. Each section delimited by two horizontal lines corresponds to a different model in the following order: LTF STD-L0, LTF STD-L10, LTF STD-L20, LTF 150-L20, LTF 50/RG-L20, LTF SCREW-L20, LTH WHD-L10.

β	Step 1	Step 2	Step 3	Step 4	Step 5	Step 6	Step 7	Step 8	Step 9	Step 10	Step 11	Step 12	Step 13	Step 14	Step 15	Step 16	Step 17	Step 18	Step 19	Step 20
β_1	150.80	-257.70	-299.43	-287.89	-368.46	-346.59	-430.67	-322.48	-466.10	-338.35	-304.94	-251.28	-153.86	28.21	-138.15	80.66	43.12	280.97	-12.92	-69.51
β_2	342.82	346.80	379.38	372.46	489.07	463.72	598.26	512.05	818.18	712.75	683.97	319.23	610.72	393.62	409.08	-62.41	110.03	195.39	249.76	320.24
β_3	154.54	-280.01	-312.30	-300.92	-405.58	-386.30	-535.99	-468.13	-736.09	-741.56	-704.68	-349.19	-617.85	-607.27	-396.40	-198.97	-331.62	-234.80	-180.36	-293.62
β_4	61.87	78.27	-4.36	2.10	13.15	0.50	44.19	-1.55	153.90	10.58	8.07	-325.51	61.32	17.47	169.00	-162.81	276.68	11.23	145.75	237.75
β_5	14.90	-23.34	-12.30	-13.83	-9.80	-14.67	26.94	-9.06	-12.50	-20.76	-10.16	342.91	-50.31	161.97	-196.77	-26.26	-164.98	-416.36	-104.17	-284.05
β_6	39.00	-24.45	-1.87	2.94	1.38	3.75	-3.63	9.31	-30.91	-3.67	-5.06	-23.09	23.34	-203.44	-20.60	272.18	-231.89	34.94	47.53	-23.01
β_7	-171.21	-111.06	-158.75	-174.44	-207.82	-241.89	-237.78	-325.76	-379.66	-287.84	-547.00	-180.57	-102.54	-419.83	-479.72	0.00	-191.46	-352.69	0.00	-391.54
β_8	-201.01	-111.72	-167.54	-181.25	-228.37	-249.34	-264.00	-341.96	-320.20	-445.17	-436.41	-246.91	-380.53	-451.85	0.00	-23.74	-229.86	91.51	-40.32	0.00
β_1	-100.38	-168.30	-162.66	-156.19	-199.63	-183.78	-195.30	-199.44	-161.01	-211.04	-144.75	-120.90	-113.68	53.17	90.81	-18.52	98.19	-205.71	-29.29	83.17
β_2	260.69	266.72	255.35	249.78	339.76	310.48	341.29	330.30	316.39	458.06	447.10	444.64	440.77	90.74	520.60	228.14	119.13	688.91	355.04	389.07
β_3	-97.46	-222.31	-222.16	-214.77	-297.83	-280.88	-304.56	-342.55	-310.16	-433.08	-467.76	-481.02	-485.35	-293.00	-386.62	-245.79	-303.52	-622.59	-64.07	-134.92
β_4	-106.89	-54.04	0.94	-5.03	-29.53	-4.49	-30.94	-10.86	-2.01	-123.99	41.27	-26.20	-35.01	251.58	-126.20	-228.23	279.55	88.04	-215.31	214.39
β_5	13.93	6.61	9.73	9.89	2.28	6.55	15.94	4.55	1.08	67.59	-2.93	25.16	31.88	-132.16	-25.84	245.70	-143.09	66.92	203.80	-309.61
β_6	-90.95	18.76	0.73	-3.73	1.99	-2.16	4.53	-19.42	-4.76	20.73	9.31	-13.56	-10.84	-169.73	-169.62	35.11	-164.03	-101.30	308.67	-266.14
β_7	-81.75	-85.46	-89.17	-106.82	-123.70	-124.59	-155.32	-108.09	-151.68	-240.47	0.77	-171.83	-224.21	-46.77	-146.43	0.00	-191.97	-61.37	0.00	-105.12
β_8	-104.50	-51.58	-72.93	-94.68	-111.12	-99.55	-150.23	-90.61	-142.58	-184.49	-57.54	-118.29	-198.70	-69.92	-35.35	-183.23	0.00	-230.72	-41.56	0.00
β_1	153.97	11.22	-95.66	-184.20	-64.45	40.33	-162.49	-74.44	-119.38	-179.46	-68.57	-248.60	8.69	77.01	-161.38	-139.38	-49.38	92.97	19.62	16.69
β_2	283.22	157.08	507.25	149.02	32.69	147.14	265.54	55.02	351.69	160.61	190.20	455.66	68.11	205.02	414.22	154.64	80.39	184.51	258.02	84.39
β_3	150.15	-95.87	-318.04	-108.32	-94.49	-123.51	-233.63	-135.83	-166.19	-138.36	-279.00	-422.38	-146.49	-196.99	-184.84	-153.68	-289.33	-231.96	-150.91	-47.48
β_4	-152.08	-121.54	258.37	117.84	-117.64	96.22	-3.27	-184.20	124.50	145.39	5.52	-29.86	205.92	-117.34	107.05	142.00	-321.83	159.45	-20.30	-38.94
β_5	-22.78	-108.97	-241.80	-139.51	9.54	93.78	-3.36	6.65	-58.45	-153.58	-137.85	-52.15	-8.69	-130.66	-118.02	-166.32	47.88	71.07	-72.49	92.93
β_6	-152.04	36.89	155.33	4.39	106.68	-13.04	7.66	136.10	161.06	-3.25	120.92	13.00	-68.11	-2.64	239.18	-10.13	177.65	-20.47	-111.00	69.74
β_7	-138.72	-61.08	0.00	-86.81	-102.42	-71.95	-105.04	-131.90	-87.15	-138.15	-141.78	-197.30	-77.91	-120.97	0.00	-137.68	-3.93	27.84	138.27	0.00
β_8	-89.68	0.00	-52.18	0.00	-75.69	-90.14	0.00	-100.80	-104.57	0.00	-137.07	-157.93	-95.94	-55.72	-134.37	0.00	-184.47	37.81	0.00	-63.32
β_1	-890.93	-957.18	-469.28	-978.08	-964.40	-1362.64	-1242.03	-1348.49	-664.66	-1267.53	-1211.69	-2058.79	-1224.09	-450.74	-1192.55	586.59	-4.00	-81.63	-564.40	-952.74
β_2	984.91	1143.16	711.29	1282.64	1346.82	1710.39	1621.63	1983.75	1140.48	2209.28	1658.10	3043.49	2090.81	1195.48	1633.90	1718.94	524.55	429.45	1108.40	549.57
β_3	-1069.61	-1099.57	-1185.36	-1129.53	-1197.75	-1522.30	-1438.90	-1763.17	-2070.73	-2151.34	-1575.44	-3039.67	-1952.12	-1808.51	-1396.72	-1047.69	-257.91	-151.63	-248.94	-167.48
β_4	139.55	-372.51	-5.58	-24.24	-103.64	-20.98	11.49	-331.83	-66.64	-331.78	161.97	-451.72	-79.99	69.11	-215.33	-87.07	-363.51	365.88	-455.55	-473.71
β_5	45.60	49.52	569.46	33.78	115.07	-52.83	-12.14	208.40	863.33	340.18	-175.13	82.80	45.79	-849.63	193.03	1680.51	-426.96	378.47	120.86	243.34
β_6	114.05	-26.01	-611.11	-16.75	-18.46	16.71	-0.97	40.71	-941.81	17.19	-0.11	169.00	-52.73	796.60	5.63	548.17	101.60	-132.61	-357.80	-56.63
β_7	-599.19	-369.55	-687.27	-715.33	-783.73	-980.64	-1074.35	-1144.04	-1159.48	-1472.94	-1608.30	-1049.59	-1621.23	-1966.73	-2006.24	1002.47	-48.94	0.00	-191.56	0.00
β_8	-610.58	-376.57	-622.64	-743.09	-821.68	-987.62	-1116.51	-1194.69	-1069.22	-1469.20	0.00	-1733.65	-5.89	-1620.61	-1912.97	109.09	0.00	201.57	0.00	18.16
β_1	-144.78	-256.77	-253.05	-249.23	-332.52	-306.58	-418.60	-290.39	-290.48	-481.49	-276.21	-258.83	11.80	51.90	-95.21	41.28	56.67	22.83	82.38	-15.93
β_2	346.90	386.62	350.69	350.52	457.18	436.71	604.20	466.68	461.63	781.50	603.50	583.16	97.53	538.28	171.59	291.83	400.52	118.11	249.69	127.45
β_3	-117.33	-294.80	-272.94	-264.78	-359.50	-339.84	-477.64	-410.26	-407.74	-708.18	-616.49	-610.91	-371.20	-365.57	-204.16	-526.89	-261.04	-71.40	-145.08	-141.98
β_4	-147.30	-52.24	4.39	-1.78	-13.90	7.94	-67.78	17.33	17.92	7.43	63.21	60.95	318.66	-102.13	-185.19	104.63	-4.74	-52.10	117.78	-123.98
β_5	12.94	-37.40	-16.87	-18.29	-34.44	-41.46	-86.68	-63.07	-71.48	-205.48	-101.32	-93.84	-150.07	-99.28	190.56	49.24	-179.37	137.41	-276.99	145.45
β_6	-114.81	42.50	20.16	12.87	19.74	23.73	74.79	32.85	34.63	90.37	7.39	-4.47	-235.80	-211.55	23.12	-201.31	-199.63	100.67	-180.48	25.42
β_7	-104.22	-108.15	-128.91	-142.93	-155.66	-188.73	-164.01	-227.27	-241.74	-206.75	-339.55	-417.44	-88.38	-229.84	0.00	-292.18	-129.01	0.00	-150.34	0.00
β_8	-139.01	-76.33	-104.96	-131.44	-147.31	-159.59	-190.84	-150.73	-221.90	-170.01	-282.29	-345.04	-133.46	59.81	-213.01	-209.62	0.00	-68.03	0.00	-121.76
β_1	-167.90	-109.12	-101.55	-169.83	-170.25	-35.40	-92.59	-86.54	-152.18	-76.61	-102.38	-90.83	8.52	49.52	-24.26	50.62	33.02	55.78	87.35	9.11
β_2	238.86	163.45	156.68	289.73	264.62	120.96	203.82	160.48	353.55	323.03	316.17	128.92	337.51	154.40	127.61	67.49	48.07	77.89	95.80	4.75
β_3	-190.77	-145.98	-143.00	-262.82	-258.31	-238.65	-234.79	-188.78	-410.90	-349.12	-372.53	-182.45	-252.34	-87.54	-148.55	-175.50	-165.75	-216.33	-187.03	5.56
β_4	3.78	3.67	1.42	-1.44	7.33	0.95	-6.08	31.20	-4.85	-5.24	24.78	-159.49	118.67	71.07	-129.23	153.98	-140.75	179.19	-169.63	4.75
β_5	-5.27	0.11	-2.97	-29.78	-23.91	68.08	2.37	-38.95	-32.96	-20.25	-21.97	151.89	-41.34	-170.87	146.93	-89.02	73.07	-115.03	126.79	5.56
β_6	10.15	0.06	1.11	3.44	15.22	-88.28	1.52	-2.74	-8.83	-23.43	1.97	-3.15	125.15	-109.09	23.08	-105.89	88.13	-137.15	135.25	8.30
β_7	-99.50	-72.79	-102.37	-155.53	-203.56	-92.39	-138.77	-170.36	-103.79	-195.41	-238.96	-43.28	-33.28	-67.34	0.00	-144.60	0.00	80.83	0.00	243.24
β_8	-103.19	-64.48	-102.96	-133.52	-202.78	-84.67	-143.54	0.00	-115.56	-71.79	-197.56	-226.59	-30.85	0.00	-103.26	0.00	-143.83	0.00	86.74	0.00
β_1	-5.61	-188.04	-245.37	-211.72	-211.23	-279.88	-257.04	-343.68	-254.50	-240.77	-368.93	-191.32	-197.44	-229.76	-105.46	-4.40	-27.91	-80.62	31.83	50.32
β_2	189.64	262.87	350.46	298.51	311.11	377.99	367.64	498.78	387.06	379.24	648.19	491.58	472.63	475.69	214.94	47.53	410.42	214.71	67.99	89.12
β_3	-38.19	-191.60	-257.23	-222.57	-237.13	-297.56	-286.00	-391.89	-347.37	-335.15	-594.34	-488.63	-496.73	-480.70	-235.73	-196.20	-288.34	-242.31	-183.45	-184.27
β_4	-11.59	33.22	34.27	2.12	16.41	8.41	0.72	82.29	-2.39	6.42	71.76	30.54	16.71	24.93	213.27	-179.08	165.16	171.74	-161.72	131.53
β_5	-20.81	6.59	2.56	-2.34	-18.48	1.64	-1.75	6.04	0.92	3.19	58.95	-7.91	-11.03	-61.04	-237.41	64.65	-91.67	-182.84	89.72	-77.09
β_6	106.23	-29.85	-18.62	-1.08	0.43	-4.81	-1.38	-29.27	-17.21	-8.93	-48.67	10.25	-1.34	23.58	-24.18	116.58	151.09	-22.05	125.87	-115.89
β_7	-177.24	-102.78	-66.98	-88.21	-116.94	-132.58	-159.96	-175.91	-130.52	-190.37	-236.15	-80.60	-218.96	-269.88	-103.12	-218.66	-179.81	-240.37	0.00	-22.95
β_8	-135.31	-64.86	-94.32	-100.00	-112.39	-129.18	-151.45	-135.73	-168.05	-198.17	-112.43	-203.03	-279.79	-85.42	0.00	-182.31	-224.67	0.00	-77.36	0.00
β_1	-95.65	-210.92	-202.33	-195.24	-253.88	-228.00	-250.34	-212.05	-205.09	-285.59	-239.89	-209.95	-201.28	7.50	-90.95	54.19	-208.60	84.98	92.11	101.95
β_2	279.81	319.82	301.56	299.68	408.03	375.46	442.74	448.92	432.09	684.35	661.36	629.02	538.50	684.53	320.66	101.14	645.87	310.02	289.42	291.28
β_3	-115.63	-265.75	-258.02	-254.25	-353.49	-337.39	-403.43	-447.02	-442.60	-678.62	-723.18	-686.53	-593.23	-499.44	-345.15	-290.89	-672.64	-153.93	-147.00	-150.31
β_4	-121.10	-46.40	5.31	2.89	-19.85	3.60	-64.43	37.40	16.57	-101.77	31.38	23.10	-55.43	248.16	316.46	-265.37	29.33	135.22	-134.54	138.31
β_5	-7.83	-28.44	-5.56	-8.16	-28.05	-8.47	31.08	-17.28	-23.71	9.05	-12.22	-23.93	52.51	-96.51	-349.35	126.67	-129.87	-328.73	301.89	-303.28
β_6	-90.18	35.05	9.63	4.77	20.49	5.19	10.03	18.00	3.23	19.60	-0.71	-4.25	-5.35	243.78	-35.95	173.63	14.69	-204.16	189.43	-186.68
β_7	-99.88	-114.60	-139.11	-142.93	-166.13	-209.44	-299.60	-155.15	-268.08	-217.70	-347.47	-454.20	-384.14	-33.22	-244.07	0.00	-352.45	-93.82	0.00	-8.23
β_8	-126.94	-67.67	-102.10	-135.89	-145.85	-153.02	-200.02	-157.79	-251.89	-300.16	-172.81	-373.90	-453.18	-99.46	0.00	-279.45	-355.88	0.00	-53.44	0.00
β_1	-140.43	-249.53	-257.70	-251.30	-325.10	-306.25	-336.21	-294.25	-271.99	-366.35	-303.51	-260.06	-251.71	-114.44	-113.95	31.70	-249.43	12.65	27.68	18.75
β_2	374.00	388.63	370.53	368.99	498.25	457.76	553.28	503.12	485.30	756.99	671.46	635.59	568.04	703.05	236.80	92.28	599.35	210.88	190.27	161.76
β_3	-141.25	-316.20	-305.75	-300.71	-417.40	-391.29	-484.02	-489.61	-473.49	-718.01	-735.19	-696.19	-633.16	-423.84	-260.75	-323.37	-600.76	-99.36	-93.62	-82.36
β_4	-148.32	-69.02	-4.87	-8.71	-41.66	-6.78	-101.15	14.27	-7.79	-159.71	1.48	-24.49	-80.77	182.59	228.66	-284.29	-48.93	86.59	-87.99	76.50
β_5	37.69	9.55	30.34	30.31	21.78	27.00	86.43	26.54	21.78	73.39	44.30	36.31	90.69	-103.67	-268.88	131.37	-54.46	-223.65	195.90	-167.62
β_6	-133.36	23.82	-4.89	-12.36	1.36	-9.49	-3.40	10.33	-2.55	30.33	14.93	2.27	3.44	355.69	-40.03	191.95	65.09	-173.29	153.93	-140.11
β_7	-111.73	-125.25	-148.20	-163.20	-180.83	-195.39	-284.81	-141.28	-223.39	-188.37	-279.81	-366.41	-322.99	-80.46	-233.72	0.00	-251.82	-96.29	0.00	-159.09
β_8	-151.60	-80.22	-125.09	-159.88	-175.37	-184.44	-238.94	-170.37	-260.72	-310.71	-167.50	-354.44	-427.73	-145.28	0.00	-294.63	-310.55	0.00	-102.26	0.00

Table 9. Parameters of the EEGBW models corresponding to the CLT tests: the 20 values derive from division of the experimental data into 20 equal segments, named steps, characterized by constant β values. Each section delimited by two horizontal lines corresponds to a different model in the following order: CLT STD-L0, CLT STD-L20, CLT NA620-L0, CLT NA620-L20, CLT ND620-L0, CLT ND620-L20, CLT NA340-L20, CLT NAWH-L20.

β	Step 1	Step 2	Step 3	Step 4	Step 5	Step 6	Step 7	Step 8	Step 9	Step 10	Step 11	Step 12	Step 13	Step 14	Step 15	Step 16	Step 17	Step 18	Step 19	Step 20
β_1	7527.64	809.33	250.72	443.60	809.83	484.49	1163.52	1503.54	833.69	2161.62	2891.32	2846.82	2776.99	-2304.28	124.82	2105.91	106.11	2142.71	201.85	1737.73
β_2	-1927.49	-207.05	32.50	-80.99	-135.18	-1.12	-19.82	-500.25	201.24	437.87	-476.41	834.42	900.08	338.81	905.36	2045.80	203.96	-494.77	77.74	-635.93
β_3	3805.33	-2177.64	-2226.48	-2161.07	-3051.28	-2990.73	-3835.43	-4214.02	-4093.80	-5766.70	-8114.64	-6986.40	-6799.85	-3078.49	-3764.17	-2561.94	-182.25	-3335.51	-391.88	-2909.69
β_4	-2925.99	378.42	1.17	90.08	321.13	96.07	908.53	-21.24	228.59	1791.84	748.64	1816.46	1803.03	-2861.61	2628.20	260.58	-106.11	2608.12	-201.85	2087.94
β_5	4803.83	3086.54	1729.22	1776.20	2585.93	1982.53	2026.17	2873.23	2003.25	2155.60	4239.63	2418.74	2252.09	1557.26	-2041.33	-776.72	523.98	-232.61	515.99	-185.82
β_6	-8406.99	-3613.37	-2460.45	-2450.71	-3464.01	-2894.89	-3649.46	-4267.59	-3356.02	-5205.65	-7187.57	-5468.02	-5417.63	-2087.41	-2821.86	-3974.59	182.25	-3954.12	391.88	-3639.16
β_7	-1261.08	-639.08	-1070.07	-1647.46	-1840.88	-1712.28	-2536.74	-972.89	-3120.79	-3665.95	-226.76	-4085.76	-5471.33	0.00	24.88	-2231.56	0.00	-2811.97	0.00	-777.31
β_8	-739.01	-783.69	-1136.01	-1274.86	-1216.89	-1644.53	-1836.90	-912.49	-1931.46	-2472.62	-952.88	-3517.86	-4244.37	-151.36	-582.40	-683.65	-1128.70	0.00	-910.61	0.00
β_1	-3.61	-4.61	3.36	4.48	5.88	10.63	12.09	21.32	39.25	36.32	78.62	99.75	3.10	-56.90	0.85	-0.75	-51.49	0.57	-1.04	64.48
β_2	10.83	5.76	9.80	8.10	10.81	15.62	16.60	33.69	41.79	40.14	93.42	104.80	4.10	-61.70	9.00	64.86	-62.25	-12.60	1.04	0.96
β_3	-2.23	-0.63	-6.45	-4.29	-6.53	-10.71	-10.84	-23.63	-33.64	-34.15	-92.58	-112.60	-115.23	-116.55	-112.35	-60.84	-112.02	-107.82	-40.98	-64.08
β_4	4.88	-1.31	0.73	-0.09	-1.70	0.23	-0.11	5.27	-2.95	-1.39	9.16	-0.60	-0.93	-3.50	-6.64	62.11	-10.69	14.01	-1.04	64.77
β_5	-0.96	3.03	-1.60	0.08	1.06	-0.18	1.31	4.14	6.05	8.02	13.25	14.52	113.53	60.65	112.26	62.09	60.84	108.13	40.98	-0.27
β_6	4.17	-4.93	-0.22	0.40	-0.79	0.70	2.05	-2.08	7.83	9.93	8.63	22.89	125.55	57.96	124.74	2.02	52.91	127.37	-40.98	65.71
β_7	-3.53	6.82	13.18	0.00	0.00	0.00	0.00	0.00	0.00	0.00	0.00	0.00	0.00	0.00	0.00	0.00	0.00	0.00	0.00	0.00
β_8	0.86	11.70	0.00	0.00	0.00	0.00	0.00	0.00	0.00	0.00	0.00	0.00	0.00	0.00	0.00	0.00	0.00	0.00	0.00	0.00
β_1	3.96	8.54	-3.12	12.79	4.02	12.36	4.31	13.34	24.94	19.82	55.74	51.37	101.70	78.32	173.12	167.16	0.18	0.51	1.39	2.47
β_2	7.27	16.00	24.42	18.87	10.04	16.51	21.68	13.46	32.21	55.75	67.22	38.77	104.32	127.21	172.42	157.27	89.29	88.65	88.52	86.58
β_3	0.18	-11.59	-25.52	-6.89	-1.67	-1.31	-15.08	-3.11	2.70	-48.20	15.95	-24.22	-64.33	-186.66	-162.31	-142.45	-79.86	-80.44	-82.35	-80.75
β_4	6.71	2.14	-6.11	6.11	0.12	-0.41	15.47	3.58	-2.63	28.09	19.33	-13.70	-13.23	38.17	3.55	11.85	87.76	-88.43	89.87	-90.42
β_5	-0.52	-12.65	3.68	-4.23	-17.79	-21.19	-28.29	-25.51	-43.11	-36.40	-34.01	-1.85	55.79	-123.92	3.35	-11.64	81.75	-81.68	83.77	-81.84
β_6	5.98	-5.19	-2.86	0.79	-12.81	-18.57	-12.29	-26.48	-38.85	-25.36	-48.10	22.77	-28.10	-81.60	-6.70	0.22	7.72	-7.48	6.13	-7.20
β_7	-3.78	-5.39	-13.94	-10.18	-26.27	-29.91	-18.70	-40.01	-46.48	-3.07	-64.18	0.00	-86.10	33.11	0.00	0.00	0.00	0.00	0.00	0.00
β_8	-2.83	1.80	-1.03	-10.75	-14.00	-5.06	-18.56	0.00	1.66	0.00	0.00	-12.65	13.45	0.00	0.00	0.00	0.00	0.00	0.00	0.00
β_1	-1.84	4.28	8.96	9.39	12.29	17.99	18.19	36.04	55.72	56.17	138.86	146.68	144.85	81.98	147.70	61.33	82.67	156.69	-1.48	1.00
β_2	1.29	7.98	11.90	11.55	14.93	20.75	20.37	46.07	58.12	57.39	155.47	147.76	145.89	-0.64	161.88	75.45	-1.09	157.75	84.03	81.87
β_3	-2.35	-8.45	-12.60	-12.20	-16.18	-20.99	-20.24	-38.05	-46.05	-47.44	-147.80	-160.82	-161.21	-83.67	-154.48	-152.27	-86.07	-169.03	-86.95	-82.88
β_4	-1.93	-2.25	-0.06	-0.13	-2.77	0.89	-0.11	5.55	-0.83	-1.67	12.01	-0.23	-0.14	-82.65	-12.97	15.25	-84.76	-0.10	84.25	-79.21
β_5	0.03	0.81	0.17	0.25	1.01	-0.83	-0.23	4.53	-2.51	-3.60	-0.16	-11.75	-16.06	0.37	-1.99	74.98	0.21	-5.59	83.76	-87.54
β_6	-2.04	-0.47	-0.57	-0.48	-1.31	-1.97	-1.63	-1.75	-2.28	-2.57	-11.82	-12.41	-16.63	-81.71	8.41	61.80	-81.79	-6.05	-1.21	4.67
β_7	1.72	7.65	0.00	0.00	0.00	0.00	0.00	0.00	0.00	0.00	0.00	0.00	0.00	0.00	0.00	0.00	0.00	0.00	0.00	0.00
β_8	2.04	0.00	0.00	0.00	0.00	0.00	0.00	0.00	0.00	0.00	0.00	0.00	0.00	0.00	0.00	0.00	0.00	0.00	0.00	0.00
β_1	-47.59	16.09	-39.72	-6.78	3.01	-39.88	-40.89	-42.99	-59.99	-43.84	-83.02	-31.12	-76.37	34.77	107.44	101.11	58.24	-0.34	-0.04	2.14
β_2	37.96	39.26	51.43	31.18	7.03	79.23	87.47	91.91	144.31	180.11	200.08	64.83	197.46	71.04	108.36	82.23	120.39	63.51	60.96	59.87
β_3	-50.28	-32.15	-66.16	-57.68	-71.26	-105.66	-123.01	-124.55	-188.87	-200.85	-233.09	-107.43	-278.74	-77.77	-94.93	-60.14	-46.59	-49.69	-52.82	-51.35
β_4	-13.99	-3.10	-10.10	0.38	-12.74	-3.31	-3.93	-5.37	16.58	-7.65	19.22	-91.25	172.12	11.10	4.35	21.59	57.84	-61.11	62.95	-64.75
β_5	-1.22	-36.14	11.19	-11.35	-46.96	5.94	-0.40	-2.11	-6.34	-22.40	6.56	81.02	-161.25	-59.43	4.10	-22.54	-10.99	-51.41	50.76	-50.75
β_6	-12.50	-12.96	-1.86	26.61	49.97	10.77	0.42	2.55	15.39	-17.69	-6.86	17.79	-2.89	-46.38	-14.80	-1.12	-46.99	-11.76	10.16	-11.26
β_7	-32.70	-30.23	-60.80	-50.35	-76.62	-87.99	-95.30	-125.69	-137.49	-104.21	-212.12	0.00	-263.86	488.94	0.00	0.00	0.00	0.00	0.00	0.00
β_8	-32.24	-20.65	-47.67	-61.82	-68.71	-76.20	-106.96	-114.02	-107.07	0.00	-154.96	-195.62	244.41	0.00	0.00	0.00	0.00	0.00	0.00	0.00
β_1	-8.41	-3.53	3.70	5.24	7.69	7.39	13.14	14.20	14.48	38.50	9.28	54.25	110.53	74.02	166.97	72.17	152.72	4.29	-1.62	-2.22
β_2	8.70	2.49	10.00	9.53	11.22	12.13	17.67	16.93	22.71	49.07	21.34	51.12	112.04	96.70	162.10	68.65	149.02	89.41	78.36	78.57
β_3	-4.44	-0.56	-6.82	-7.04	-5.80	-7.33	-10.74	-11.28	-13.04	-31.10	-11.20	-39.72	-88.26	-154.41	-155.66	-142.82	-157.36	-74.04	-81.63	-83.46
β_4	-1.04	2.74	0.46	0.97	-0.48	-2.63	-0.19	1.10	-6.01	-4.67	11.90	-7.06	-5.51	9.78	5.67	5.26	-4.23	-83.71	79.39	-80.03
β_5	-0.06	0.23	0.82	-1.92	1.72	0.45	-0.45	0.25	2.18	2.16	21.17	-3.02	31.17	-94.66	0.78	67.43	1.44	-88.31	77.36	-77.56
β_6	-1.10	-1.27	0.52	-0.44	2.82	1.07	1.04	1.19	-0.05	-7.37	9.45	7.95	-26.31	-76.06	-7.88	73.39	2.47	-5.39	-0.62	1.21
β_7	-1.14	7.45	0.00	0.00	0.00	0.00	0.00	0.00	0.00	0.00	0.00	0.00	0.00	0.00	0.00	0.00	0.00	0.00	0.00	0.00
β_8	-2.42	6.57	6.75	0.00	0.00	0.00	0.00	0.00	0.00	0.00	0.00	0.00	0.00	0.00	0.00	0.00	0.00	0.00	0.00	0.00
β_1	-3.30	2.45	7.27	7.62	9.95	14.85	14.79	27.26	42.39	43.49	90.84	107.92	109.84	57.26	108.87	36.90	60.79	115.08	-1.90	12.01
β_2	4.44	5.33	10.38	9.66	12.14	17.87	17.17	35.30	43.59	43.00	102.93	110.04	110.47	-0.10	120.61	55.42	-0.19	116.52	58.66	51.08
β_3	-1.39	-6.23	-10.38	-9.92	-13.93	-17.31	-17.15	-30.61	-38.75	-40.75	-94.59	-106.26	-108.31	-59.64	-112.56	-102.46	-63.09	-125.37	-64.23	-39.00
β_4	0.31	-3.04	-0.72	-0.56	-2.86	-0.05	-0.46	4.64	-1.21	-2.65	9.19	-0.03	-1.38	-58.30	-10.07	19.36	-63.23	0.10	59.39	-36.79
β_5	0.62	2.02	1.32	1.69	3.25	2.26	3.00	8.80	2.18	1.62	3.13	-0.62	-0.92	1.25	0.17	55.01	-0.32	-6.55	59.71	-77.31
β_6	1.20	2.04	2.10	2.71	2.46	2.85	3.05	2.42	2.59	3.58	-4.59	-0.48	0.09	-58.42	6.72	37.32	-60.28	-9.35	-2.94	14.22
β_7	1.78	7.03	0.00	0.00	0.00	0.00	0.00	0.00	0.00	0.00	0.00	0.00	0.00	0.00	0.00	0.00	0.00	0.00	0.00	0.00
β_8	1.38	0.00	0.00	0.00	0.00	0.00	0.00	0.00	0.00	0.00	0.00	0.00	0.00	0.00	0.00	0.00	0.00	0.00	0.00	0.00
β_1	-1.73	-1.25	1.72	6.28	11.24	12.46	18.09	18.72	25.06	49.83	14.29	48.48	106.23	63.81	126.35	48.38	124.72	-1.95	-7.89	-2.75
β_2	6.12	1.29	4.80	12.43	15.67	18.40	24.94	23.55	35.30	54.43	19.64	50.64	107.48	74.41	125.00	48.02	134.68	73.33	64.61	75.18
β_3	-2.05	-3.36	-3.79	-16.11	-14.57	-18.72	-25.90	-26.09	-35.37	-61.54	-56.79	-60.98	-114.98	-133.24	-146.09	-134.81	-134.14	-73.64	-82.04	-77.25
β_4	2.14	-1.25	-1.82	3.06	1.54	-0.83	2.04	2.22	-7.84	3.55	3.72	0.32	-1.87	-1.42	7.08	5.59	7.33	-70.98	69.22	-73.84
β_5	-1.22	2.24	7.30	-5.84	0.49	0.13	-4.18	-3.52	-0.79	-10.25	19.06	-12.57	-5.44	-73.20	-20.30	44.71	-10.13	-72.10	61.65	-73.09
β_6	-3.17	-3.36	-6.32	-8.45	-3.54	-7.33	-6.86	-8.02	-10.11	-14.25	14.88	-13.37	-20.29	-65.03	-26.15	51.69	-17.18	0.71	-4.93	0.66
β_7	-5.24	7.56	18.90	0.00	0.00	0.00	0.00	0.00	0.00	0.00	0.00	0.00	0.00	0.00	0.00	0.00	0.00	0.00	0.00	0.00
β_8	1.15	0.00	0.00	0.00	0.00	0.00	0.00	0.00	0.00	0.00	0.00	0.00	0.00	0.00	0.00	0.00	0.00	0.00	0.00	0.00

Table 10. Parameters of the fragility functions

Test	**Mass** [kg]					
	1000		1500		2000	
	Parameters					
	$\hat{\theta}$	$\hat{\beta}$	$\hat{\theta}$	$\hat{\beta}$	$\hat{\theta}$	$\hat{\beta}$
LTF STD-L20	1.52472	0.60146	1.56404	0.84287	1.54906	1.04518
LTF STD-L10	1.63229	0.62631	1.56404	0.84287	1.51708	0.97519
LTF STD-L0	1.50289	0.67247	1.60632	0.98711	1.32335	1.06565
LTF 2F-L20	1.66182	1.12543	1.13099	1.04892	0.94046	1.23108
LTF 150-L20	1.54439	0.63868	1.51336	0.81990	1.44122	1.00044
LTF 50/RG-L20	1.52472	0.60146	1.56404	0.84287	1.50658	0.99728
LTF 50-L20	1.68512	0.91134	1.56371	1.09831	1.23364	1.06459
LTF SCREW-L20	1.52472	0.60146	1.56404	0.84287	1.50658	0.99728
LTF WHD-L20	1.58907	0.82071	1.62118	1.12732	1.27582	1.10323
CLT STD-L0	1.64713	0.97919	1.32888	1.07196	1.03860	1.12669
CLT STD-L20	1.59515	0.92868	1.38084	1.11367	1.05175	1.12880
CLT NA620-L0	1.57077	1.15226	1.02636	1.07841	0.82412	1.21855
CLT NA620-L20	1.46646	1.09408	1.02636	1.07841	0.81109	1.23838
CLT ND620-L0	1.63029	1.18336	1.05933	1.05522	0.85131	1.15826
CLT ND620-L20	1.66182	1.12543	1.13099	1.04892	0.88719	1.19226
CLT NA340-L20	1.51558	0.72482	1.60654	1.04925	1.27510	1.04529
CLT NAWH-L20	1.51558	0.72482	1.60654	1.04925	1.27510	1.04529